

Title: Temporal analysis of enhancers during mouse brain development reveals dynamic regulatory function and identifies novel regulators of cerebellar development.

Authors: Miguel Ramirez^{1,2}, Yuliya Badayeva^{1,2}, Joanna Yeung^{1,2}, Joshua Wu^{1,2}, Erin Yang^{1,2}, FANTOM 5 Consortium³, Brett Trost⁴, Stephen W. Scherer⁴, Daniel Goldowitz^{1,2*}

Author Affiliations: 1. Centre for Molecular Medicine and Therapeutics, BC Children's Hospital Research Institute, Vancouver, BC, Canada V6H 3V5; 2. University of British Columbia, Vancouver, BC, Canada V6T 1Z4; 3. RIKEN, 2-1 Hirosawa, Wako, Saitama 351-0198, Japan; 4. The Centre for Applied Genomics, The Hospital for Sick Children, Toronto, ON, Canada M5G 0A4

Corresponding Author: Daniel Goldowitz, Centre for Molecular Medicine and Therapeutics, BC Children's Hospital Research Institute, 950 W 28th Ave, Vancouver, BC, Canada V6H 3V5

Classification: Biological Sciences, Developmental Biology

Keywords: Enhancers, Brain development, Gene expression regulation, Epigenetics, Transcription factors, Mouse, Autism Spectrum Disorder

1 **Abstract**

2 In this study, we identified active enhancers in the mouse cerebellum at embryonic and
3 postnatal stages establishing the first catalog of enhancers active during embryonic cerebellum
4 development. The majority of cerebellar enhancers have dynamic activity between embryonic
5 and postnatal development. Cerebellar enhancers were enriched for neural transcription factor
6 binding sites with temporally specific expression. Putative gene targets displayed spatially
7 restricted expression patterns, indicating cell-type specific expression regulation. Functional
8 analysis of target genes indicated that enhancers regulate processes spanning several
9 developmental epochs such as specification, differentiation and maturation. We use these
10 analyses to discover one novel regulator and one novel marker of cerebellar development:
11 *Bhlhe22* and *Pax3*, respectively. We identified an enrichment of *de novo* mutations and variants
12 associated with autism spectrum disorder in cerebellar enhancers. Our study provides insight into
13 the dynamics of gene expression regulation by enhancers in the developing brain and delivers a
14 rich resource of novel gene-enhancer associations providing a basis for future in-depth studies in
15 the cerebellum.

16 17 **Introduction**

18 Neuronal development is a complex and dynamic process that involves the coordinated
19 generation and maturation of countless cell types. For the most numerous neuron in the brain, the
20 cerebellar granule cell, neuronal differentiation consists of several steps beginning with the
21 commitment of neural stem cells to become specified neural precursors, followed by multiple
22 migratory stages to reach and mature at its final destination (Consalez, Goldowitz, Casoni, &
23 Hawkes, 2021). Underpinning these events is the expression of gene regulatory networks that
24 drive dynamic molecular processes required for proper brain formation (Ziats, Grosvenor, &
25 Rennert, 2015). However, the transcriptional mechanisms that precisely regulate these gene
26 expression programs have not been fully described.

27 Gene expression is typically activated when transcription factors (TFs) bind to non-
28 coding regulatory elements and recruit the necessary components to begin transcription. Among
29 the several classes of non-coding sequences that regulate gene expression, enhancers are the
30 most common, with thousands predicted to coordinate transcriptional regulation during
31 development (Heinz, Sven, Romanoski, Benner, & Glass, 2015). Enhancers are stretches of DNA

32 that bind to TFs and upregulate distal target gene expression. In the brain, enhancers help to
33 ensure that gene expression is spatially- and temporally-specific, defining what genes will be
34 active during distinct stages of development (Nord & West, 2020). Transcriptional regulation by
35 enhancers has been shown to be critical for cellular identity, maturation during central nervous
36 system (CNS) development, and activity-dependent responses in mature neurons (Frank et al.,
37 2015; Pattabiraman et al., 2014). A detailed understanding of the enhancers that govern changes in
38 gene expression during embryonic and early postnatal brain development remains limited.
39 Profiling genome-wide enhancer activity at different time points and identifying their gene
40 regulatory targets can provide insight into developmental processes regulated by enhancer
41 elements.

42 Several molecular properties have been associated with enhancer activity, and the
43 advancement of sequencing technology has facilitated their identification genome-wide in
44 several developing brain structures (Carullo & Day, 2019). Enhancers are marked with histone
45 post-translational modifications H3K4me1 and H3K27ac, both of which contribute to opening
46 chromatin for TF binding (Calo & Wysocka, 2013). H3K27ac delineates active from poised
47 elements, and has been a reliable marker for enhancer activity genome-wide (Creyghton et al.,
48 2010). Analysis of these marks, in conjunction with transcriptomic and epigenomic datasets, has
49 revealed that the vast majority of non-coding variants associated with neurological and
50 psychiatric disorders are found within these regulatory elements, highlighting their importance in
51 functional readout in the brain (Barešić, Nash, Dahoun, Howes, & Lenhard, 2020). Thus, profiling
52 enhancer-associated histone modifications in the brain across time provides a comprehensive
53 understanding of gene-regulatory principles, disease-associated variants, and the genetics of
54 brain development (Nott et al., 2019).

55 The cerebellum has been a long-standing model to study the developmental genetics of
56 the brain. This is, in part, due to the limited number of cell types, well-defined epochs of
57 development for these cell types and a simple trilaminar structure in which these cells are
58 organized, making for an enhanced resolution of events in time and space (Wang, V. Y. & Zoghbi,
59 2001). More recently, the study of cerebellar development has gained added interest through its
60 documented role in the etiology of ASD (Stoodley & Limperopoulos, 2016). Previously, we
61 developed a 12-timepoint transcriptional analysis of the developing cerebellum leading to the
62 discovery of novel TFs critical for proper development (Zhang, P. G. Y. et al., 2018). More

63 recently, the developing cerebellum has served as an ideal setting for pioneering single-cell
64 RNA-seq time course studies (Carter et al., 2018; Peng et al., 2019; Wizeman, Guo, Wilion, & Li,
65 2019). At the level of gene expression regulation, chromatin accessibility and enhancer activity
66 have been examined previously in the postnatal cerebellum, leading to the discovery of distinct
67 transcriptional profiles between immature and mature neurons, coordinated by non-coding *cis*-
68 regulatory sequences (Frank et al., 2015). However, a comprehensive atlas of enhancers defining
69 the role they play during embryonic and early postnatal cerebellar development has yet to be
70 established. Profiling these non-coding regulatory elements and their target genes will discover
71 novel genetic drivers of the precisely-timed and cell-specific molecular events in the developing
72 cerebellum.

73 We utilize chromatin immunoprecipitation followed by sequencing (ChIP-seq) of
74 enhancer associated histone marks H3K4me1 and H3K27ac at 3 stages of embryonic and early
75 postnatal cerebellar development. We identify temporally specific enhancers using a differential
76 peak analysis comparing postnatal and embryonic timepoints. Transcription factor motif
77 enrichment and prediction of gene targets led to the elucidation of molecular processes regulated
78 by enhancers during these stages. We use these analyses to discover two novel regulators of
79 cerebellar development, Pax3 and Bhlhe22: a novel marker of GABAergic progenitors and a
80 regulator of postnatal granule cell migration, respectively. Finally, we identify an enrichment of
81 autism spectrum disorder (ASD) associated SNPs and *de novo* variants found in ASD-affected
82 individuals in cerebellar enhancers, functionally annotating ASD-associated variation. Our study
83 provides further insight into the dynamics of gene expression regulation by enhancers in the
84 developing brain and delivers a rich resource to help understand the developmental and
85 functional genetics of the developing cerebellum.

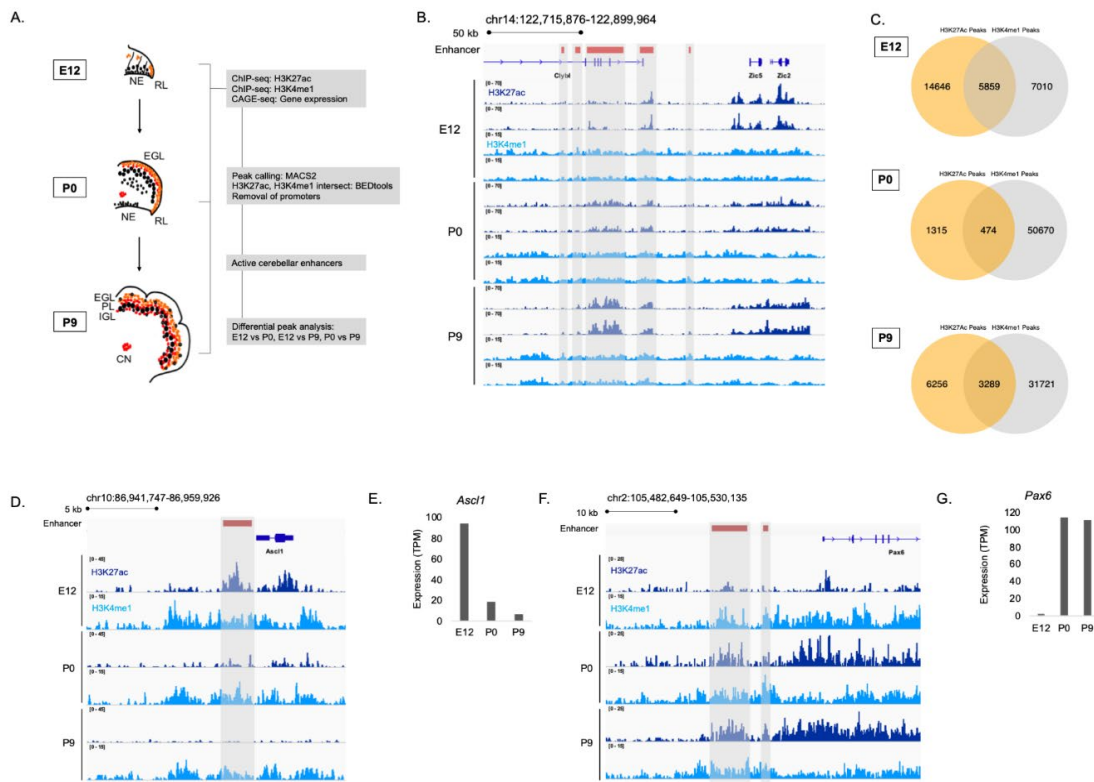
86

87 **Results**

88 **Enhancer identification during cerebellar development**

89 To identify enhancers active during embryonic and postnatal cerebellar development, we
90 generated genome-wide H3K27ac and H3K4me1 ChIP-seq profiles from mouse cerebella
91 dissected at embryonic day 12 (E12), postnatal day 0 (P0) and postnatal day 9 (P9) (**Figure 1A**).
92 These developmental days represent 3 distinct stages of murine cerebellar development, each
93 with its own developmental profile (Goldowitz & Hamre, 1998). H3K27ac and H3K4me1 signals

94 were reproducible between biological replicates as exemplified in a region on chromosome 14
 95 (**Figure 1B**). There was a high correlation between replicates for both marks at each age
 96 (**Supplementary Figure 1A**). Therefore, we had confidence in using our H3K27ac and
 97 H3K4me1 data in downstream analyses. Robust cerebellar enhancers were identified by the
 98 presence of overlapping peaks between the two enhancer-associated histone marks at each age.
 99 This highlighted a total of 9,622 peaks; 5,859, 474, and 3,289 peaks that were in both the
 100 H3K27ac and H3K4me1 datasets at E12, P0, and P9, respectively (**Figure 1C**). Duplicate peaks
 101 between ages were removed, producing a list of **7,024** active cerebellar enhancers derived from
 102 overlapping H3K27ac and H3K4me1 signals (Supplementary Data 1).
 103



104

105 **Figure 1. Enhancer identification during cerebellar development.** **A)** An overview of the stages of cerebellar
 106 development profiled in this study. The datasets collected at these ages and the downstream analyses are shown.
 107 Labels: NE: Neuroepithelium, RL: Rhombic lip, EGL: External granular layer, PL: Purkinje layer, IGL: Inner
 108 granular layer, CN: Cerebellar nuclei **B)** A region of the mouse genome chr14:122,715,876-122,899,964 (mm9) in
 109 the Integrative Genomics Viewer (IGV) showing H3K27ac and H3K4me1 profiles across biological replicates of
 110 E12, P0, P9 cerebella. Active cerebellar enhancers are highlighted (gray box). **C)** Venn diagrams displaying overlap
 111 between H3K27ac and H3K4me1 peaks at each E12, P0 and P9. **D-E)** An example of a cerebellar enhancer
 112 identified from the E12 cerebella. Shown is normalized H3K27ac and H3K4me1 signal at the enhancer (gray box),
 113 as well as **(E)** normalized CAGE-seq expression of the nearest gene, *Ascl1*, across developmental time, at E12, P0,
 114 P9. TPM, Transcripts Per Million. **(F-G)** An example of a cerebellar enhancer identified from the P9 cerebella.
 115 Shown is normalized H3K27ac and H3K4me1 signal at the enhancer (gray box), as well as **(G)** normalized (TPM)
 116 CAGE-seq expression of the nearest gene, *Pax6*, across developmental time, at E12, P0, P9.

117 The relationship between enhancer activity and genes relevant to cerebellar development
118 is shown in genomic regions flanking *Ascl1* and *Pax6*, two genes critical to cerebellar
119 development (Kim, Battiste, Nakagawa, & Johnson, 2008; Yeung, Ha, Swanson, & Goldowitz, 2016b).
120 We identified an enhancer active at E12 located in close proximity to *Ascl1* (**Figure 1D**). A
121 decrease in the H3K27ac ChIP-seq signal at this enhancer corresponded to a decrease in *Ascl1*
122 gene expression (**Figure 1E**). We identified two active enhancers at P9 located near *Pax6*
123 (**Figure 1F**). H3K27ac ChIP-seq signal also showed a pattern of activity similar to *Pax6*
124 expression, increasing from embryonic to postnatal ages (**Figure 1G**). These results provide
125 validation for the enhancers identified in our dataset in regulating genes critical to cerebellar
126 development.

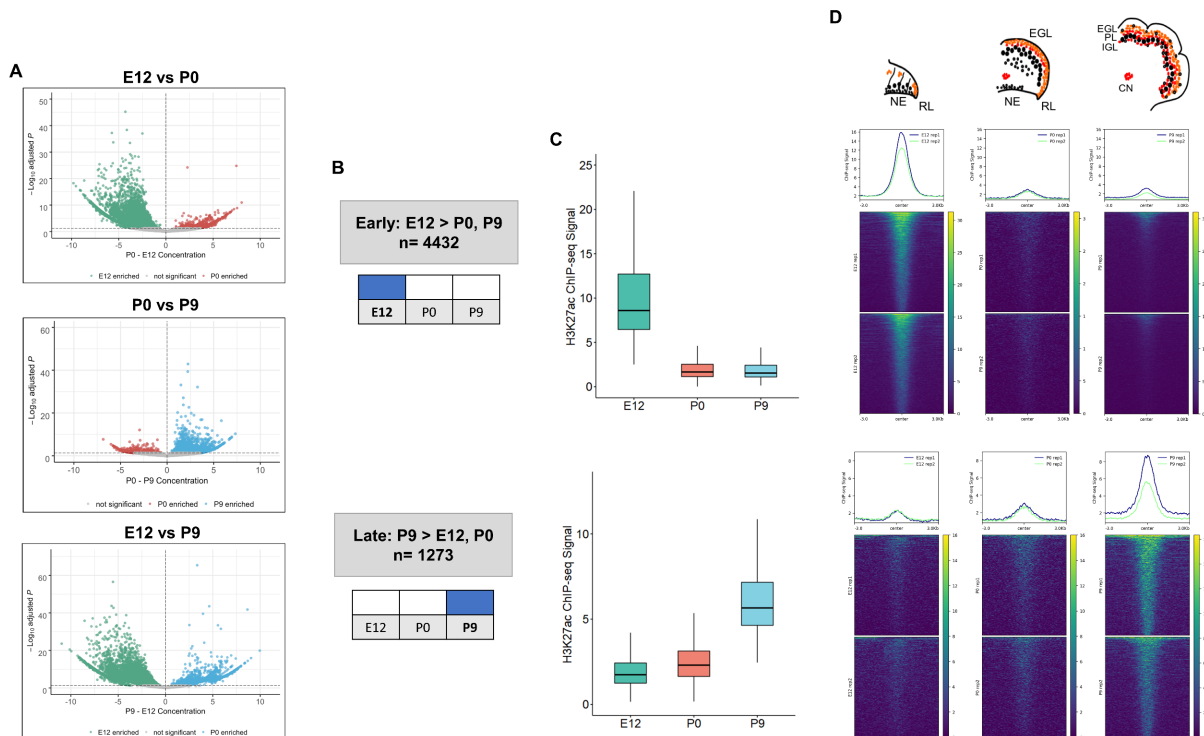
127 We compared our list of robust cerebellar enhancers to three previously published
128 enhancer datasets. First, P7 H3K27ac ChIP-seq and DNase-seq profiles previously generated by
129 Frank et al (2015) were compared to robust cerebellar enhancers. Greater than 90% of our
130 reported cerebellar enhancers are replicated by H3K27ac and DNase-seq peaks from this study
131 (**Supplementary Figure 1B-C**). Second, enhancers retrieved from the enhancer database
132 EnhancerAtlas 2.0, reporting enhancer activity in the mouse cerebellum at P0-P14 (Gao & Qian,
133 2020), were compared to robust cerebellar enhancers were compared to. We found that 73%, and
134 80% of our enhancers overlapped with the postnatal cerebellum enhancer dataset at P0, and P9,
135 respectively (**Supplementary Figure 1D**). Third, mouse enhancers that had experimentally
136 validated hindbrain activity at E11.5 from the VISTA Enhancer Browser (Visel, Minovitsky,
137 Dubchak, & Pennacchio, 2007) were compared to cerebellar enhancers. We found that 56% of
138 VISTA enhancers overlap with our cerebellar enhancer sequences at E12 (**Supplementary**
139 **Figure 1E**). These confirmative findings indicate our approach was effective in capturing active
140 cerebellar enhancers.

141

142 **Enhancer dynamics during cerebellar development**

143 The dynamics of enhancer activity over cerebellar development were examined through a
144 differential peak analysis of H3K27ac signal. The majority, **89% (6238/7023)**, of cerebellar
145 enhancers had significant differences in peak signal (adjusted p-value ≤ 0.05) throughout
146 cerebellar development (**Figure 2A**). At P9, **1273** cerebellar enhancers were significantly active
147 compared to either P0 or E12 (Supplementary Data 2). At E12, **4432** active enhancers were

148 differentially active compared to either P9 or P0 (Supplementary Data 2). At P0, in contrast, only
 149 a small number of enhancers with differential signal was identified (403 and 154 showed
 150 significant changes when compared to E12 and P9, respectively). However, none of these P0
 151 cerebellar enhancers were differentially active when compared to both E12 and P9, indicating
 152 that enhancer activity did not spike at birth. Taken together, this analysis highlights two
 153 temporally specific windows of enhancer activity at Early (embryonic) and Late (postnatal)
 154 stages (**Figure 2B**).



155
 156 **Figure 2. Enhancer activity is dynamic throughout cerebellar development.** **A)** Volcano plots showing robust
 157 cerebellar enhancers with differential H3K27ac peak signal for three comparisons: E12 vs P9, E12 vs P0, and
 158 P0 vs P9. Differential signal strength was identified for 4433 and 4355 robust cerebellar enhancers when comparing E12
 159 to P9 and to P0, respectively. At P9, 1275 and 403 robust cerebellar enhancers had differential signal when
 160 compared to E12 and P0, respectively. Enhancers with significant differential activity are colored at a cutoff of an
 161 adjusted p-value < 0.05. Displayed on the y-axis is the negative log₁₀ adjusted p-value and on the x-axis is the
 162 difference in ChIP-seq signal between to the ages for a given peak. **B)** A diagram displaying how Early and Late
 163 active cerebellar enhancers were classified based on differential peak analysis results. **C)** A boxplot showing mean
 164 ChIP-seq signal (y-axis) for all Early (upper) and Late (lower) active enhancers. Error bars represent the standard
 165 error of the mean. **D)** Mean profile and heatmaps of H3K27ac signal at the midpoint of our predicted cerebellar
 166 enhancers (rows ± 3kb) in Early and Late groups at E12, P0 and P9.

167
 168
 169 Distinct patterns of enhancer activity were observed for temporally classified enhancers.
 170 For Early active enhancers, there was a loss of mean H3K27ac signal over time, with a steep
 171 decline after E12 (**Figure 2C**). Late active enhancers exhibited a gain in activity over time, with

172 mean H3K27ac signal increasing steadily through development. These patterns are seen when
173 looking at the changes in signal flanking the summits of our peaks across time (**Figure 2D**).
174 These results indicate that the majority of cerebellar enhancers are dynamic throughout time and
175 exhibit temporally specific activity.

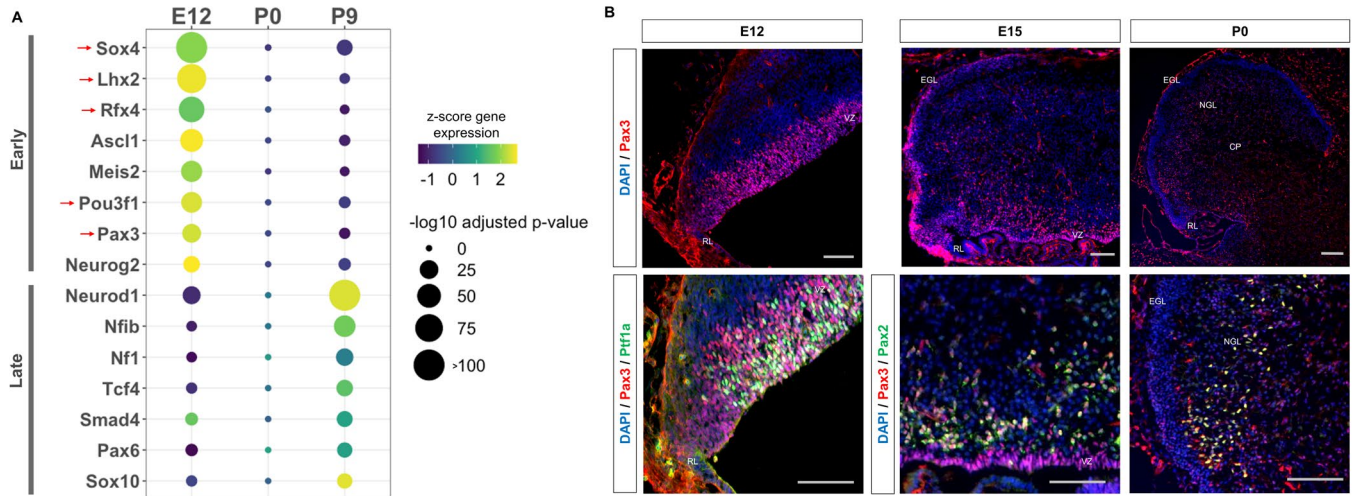
176

177 **Cerebellar enhancers are enriched for neural transcription factor binding sites in an age-** 178 **dependent manner**

179 We then sought to identify transcription factors whose activity is dictated by the
180 availability of robust cerebellar enhancers, as many neural lineage-defining factors drive cell
181 commitment in the developing brain through enhancer binding (Elsen et al., 2018; Lindtner et al.,
182 2019). We used HOMER to search for enriched motifs (adjusted p-value < 1E-11) in Late and
183 Early active cerebellar enhancers and then matched them to known transcription factor motifs in
184 the JASPAR database (Heinz, S. et al., 2010). This analysis revealed a distinct set of significantly
185 enriched motifs for Early and Late enhancers matching predicted TFs with both known and novel
186 regulatory roles in cerebellar development (**Figure 3A**). TFs enriched in the Early active
187 enhancers show a decrease in expression over time while TFs enriched in the Late active
188 enhancer group show an increase in expression over time. This correspondence between enriched
189 TF expression and enhancer activity provides validation for our findings and indicates the timing
190 of enhancer activity may be dictated by the expression and binding of these enriched TFs.

191 The top three enriched TF motifs for Early active enhancers were *Ascl1*, *Meis2* and
192 *Atoh1* (**Figure 3A**). These TFs have established roles in cerebellar development, acting as
193 markers of GABAergic or glutamatergic cell types and regulators of differentiation (Ben-Arie et
194 al., 1997; Kim et al., 2008; Wizeman et al., 2019). Importantly, many of the motifs enriched in the
195 Early group matched with TFs which have received little to no attention in the cerebellum,
196 including *Sox4*, *Lhx2*, *Rfx4*, *Pou3f1* and *Pax3* (**Figure 3A**). These TFs have been previously
197 associated with the development of other brain areas (Frantz, Bohner, Akers, & McConnell, 1994;
198 Porter et al., 1997; Su et al., 2016; Zhang, D. et al., 2006). In contrast, the TFs matching the motifs
199 enriched in the Late active enhancers have a previously identified role in cerebellar development;
200 but not necessarily involved in the same processes (**Figure 3A**). For example, the top 3 enriched
201 motifs matched with *Neurod1*, *Nfia/b/x*, and *NF1*, which have all been associated with granule
202 cell differentiation (Miyata, Maeda, & Lee, 1999; Sanchez-Ortiz et al., 2014; Wang, W. et al., 2007).

203 However, two other TFs with enriched binding sites, Pax6 and Smad4 have been found to be
 204 critical for granule cell precursor proliferation, a process preceding differentiation (Swanson &
 205 Goldowitz, 2011). These results suggest a dynamic role for the majority of our Early and Late
 206 active enhancers, driven by TFs involved in distinct stages of neuron development.
 207



208
 209 **Figure 3. Neural transcription factors with known and novel function in the developing cerebellum are**
 210 **enriched in dynamic cerebellar enhancers.** **A)** Dot plot displaying significantly enriched (adjusted p-value < 1E-
 211 11) motifs and the predicted matching transcription factor (TF). Displayed are the results for Early (top) and Late
 212 (bottom) active enhancers. TFs with an unknown functional role in cerebellar development are indicated with a red
 213 arrow. Size of the dots indicate the negative log10 adjusted p-value for a given motif and the color scale displays the
 214 z-score normalized expression throughout the cerebellar developmental time course. **B)** Top: Immunofluorescent
 215 staining of Pax3 in the mouse cerebellum at E12, E15 and P0. Bottom: Pax3 and Ptf1a immunofluorescent co-
 216 staining of the E12 mouse cerebellum. Immunofluorescent co-staining of Pax3 and Pax2 in the mouse cerebellum at
 217 E15 and P0. Labels: CP: Cerebellar parenchyma, EGL: External granular layer, NGL: Nascent granular layer, RL:
 218 Rhombic lip, VZ: Ventricular zone, Scalebars = 100um.
 219

220 **Early active enhancers are enriched for Pax3 binding sites, a novel marker for GABAergic**
 221 **cells**

222 The TF motif enrichment analysis of Early enhancers led to the discovery of several TFs
 223 with novel in the context of embryonic cerebellar development; potentially involved in seminal
 224 aspects of development such as cellular specification or commitment. As a case study, we
 225 focused on Pax3, as other members of the Pax protein family have been shown to play key roles
 226 in the developing cerebellum (Leto et al., 2009; Urbánek, Fetka, Meisler, & Busslinger, 1997; Yeung,
 227 Ha, Swanson, & Goldowitz, 2016a). Indeed, we observed robust expression in the ventricular zone
 228 (VZ); a neural progenitor region for GABAergic cells in the cerebellum (Leto, Carletti, Williams,

229 Magrassi, & Rossi, 2006) (**Figure 3B**). Colocalization between Pax3 and Ptf1a, the GABAergic
230 lineage-defining molecule in the cerebellum (Hoshino et al., 2005), confirmed expression within
231 GABAergic neural progenitors. At E15, Pax3⁺ cells are seen in the region just dorsal to the VZ,
232 which consist of post-proliferative cells such as Purkinje cells and interneurons (Hoshino et al.,
233 2005; Leto et al., 2006) (**Figure 3B**). We examined Pax3 co-labeling with markers for these cell
234 types Foxp2 and Pax2, respectively (Fujita et al., 2008; Maricich & Herrup, 1999). While
235 colocalization between Pax3 and Pax2 was found (**Figure 3B**), no co-staining between Pax3 and
236 Foxp2 was observed (**Supplemental Figure 3A**). These results extend to P0, where Pax3⁺ cells
237 are found in the nascent granule cell layer as well as the cerebellar parenchyma; ie co-labeling
238 with Pax2 and not Calbindin, a Purkinje cell marker (**Figure 3E, Supplemental Figure 3B**).
239 Thus, Pax3 is a novel marker for GABAergic progenitors and interneuron precursors in the
240 developing cerebellum.

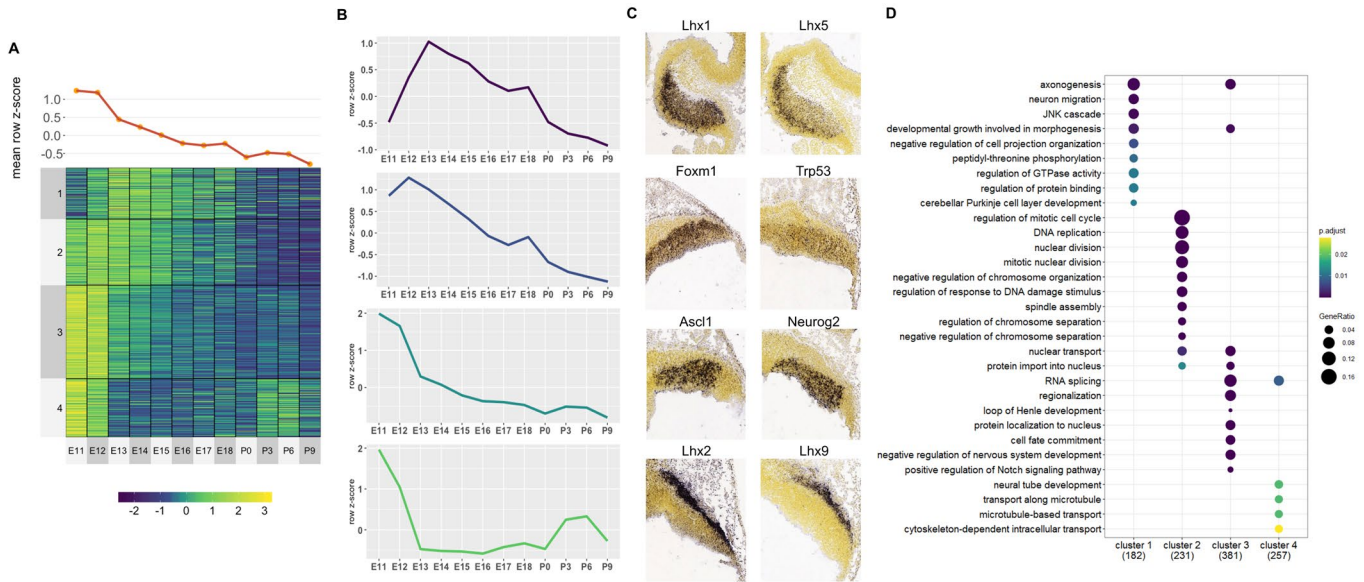
241

242 **Co-expressed putative target genes are expressed in spatially distinct areas of the** 243 **developing cerebellum.**

244 We next investigated the molecular processes regulated by robust cerebellar enhancers
245 through predicting their downstream targets (Osterwalder et al., 2018; Yao et al., 2015). This was
246 done by calculating the correlation between H3K27ac signal and gene expression at E12, P0, and
247 P9 (Zhang et al., 2018) for genes located within the same conserved topological associating
248 domain (TAD) identified previously (Dixon et al., 2012) (See Methods). Overall, at least one
249 positively correlated target gene was identified for **5815/7023 (70.61%)** cerebellar enhancers
250 with an average Pearson correlation coefficient of **0.86** (Supplementary Data 3). In total, we
251 identified **2261** target genes. Using the Mouse Genome Informatics (MGI) database, we
252 identified **98** target genes that when knocked out result in a cerebellar phenotype; demonstrating
253 the validity of our high throughput approach.

254 An unbiased *k-means* clustering was then conducted for Early and Late target genes to
255 delineate them into the various co-expression programs coordinating molecular events during
256 development. For this analysis, the target gene expression time course was expanded to 12
257 different timepoints during cerebellar development, quantified previously by CAGE-seq (Zhang
258 et al., 2018). For Early active enhancers, 4 Clusters of co-expressed target genes were identified
259 (**Figure 4A**). Genes in these clusters had decreased expression over time, similar to their

260 corresponding enhancer activity. However, a distinct mean expression profile was observed for
 261 each Cluster (**Figure 4B**). Interestingly, genes with known function during cerebellar
 262 development showed distinct spatial expression patterns, observed using ISH data from the
 263 Developing Mouse Brain Atlas (Thompson et al., 2014) (**Figure 4C**).
 264



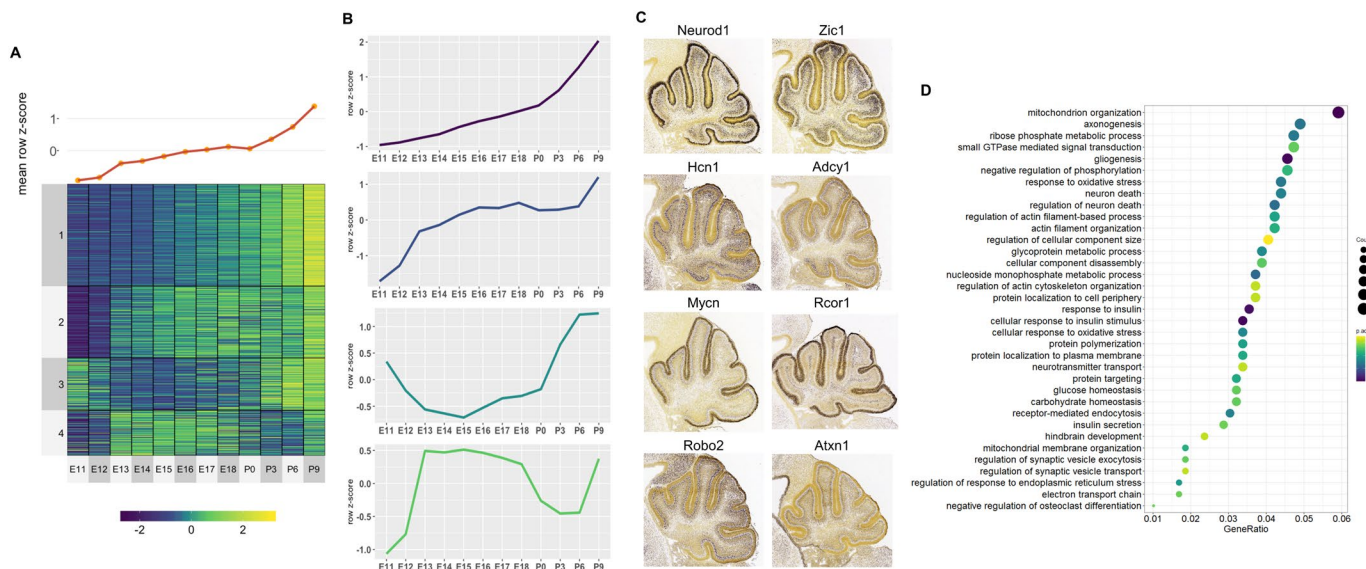
265

266 **Figure 4. Co-expressed Early target genes are expressed in spatially distinct areas and have diverse roles in**
 267 **cerebellar development.** **A)** Line plot and heatmap showing mean z-score expression for Early target genes
 268 throughout the cerebellar time course. **B)** Line graph representation of expression pattern throughout time for each
 269 cluster. **C)** Known cerebellar genes in each cluster and *in situ* hybridization (ISH) images showing spatial expression
 270 at peak expression ages. ISH images were taken from the Developing Mouse Atlas conducted at E13.5 for clusters 1
 271 and 2, and E11.5 for clusters 3 and 4. **D)** Gene Ontology (GO) enrichment analysis of target genes from each cluster,
 272 displaying the top enriched GO terms. Size of the dots indicates the gene ratio for a given cluster which is equal to
 273 the number of genes within the GO category divided by the total number of genes in the cluster. Color scale
 274 indicates the adjusted p-value for each GO term.

275 For example, in **Cluster 3**, cerebellar genes *Ascl1* and *Neurog2* are expressed exclusively
 276 in the ventricular zone at E11.5 while **Cluster 4** contains *Lhx9* and *Meis2* which are expressed in
 277 the Nuclear Transitory Zone (neurons destined for the cerebellar nuclei). A Gene Ontology (GO)
 278 enrichment analysis revealed that each cluster is enriched for molecular processes known to be
 279 regulated by cerebellar genes within the cluster (**Figure 4D**). For example, **Cluster 1** is enriched
 280 for **axonogenesis** (GO:0007409, p-value: 3.31E-4), **neuron migration** (GO:0001764, p-value:
 281 3.3E-4) and **Purkinje layer development** (GO:0021691, p-value: 0.01) and also contains *Lhx1*
 282 and *Lhx5* which are expressed in migrating Purkinje cells in cerebellar parenchyma and has
 283 previously been associated with the regulation of Purkinje cell differentiation during embryonic

284 cerebellar development (Zhao et al., 2007). Together, these findings support the notion that Early
 285 active enhancers regulate their targets in a spatially-specific manner, regulating distinct processes
 286 in their respective cell types.

287 For the Late active enhancers, 4 Clusters of co-expressed target genes were identified
 288 (Figure 5A). We observed relatively distinct expression patterns in each of the 4 Clusters with a
 289 gradual rise in mean expression throughout time (Figure 5B). Genes with known function during
 290 cerebellar development also show distinct spatial expression patterns, identified using the
 291 Developmental Mouse Atlas (Figure 5C). For example, Cluster 1 and 3 contained known
 292 cerebellar genes critical for granule cell development, such as *Neurod1* and *Zic1*, while Cluster
 293 2 and 4 contained cerebellar genes important for in Purkinje cell development, such as *Atxn1* and
 294 *Hcn1* (Figure 5C) (Aruga & Millen, 2018; Ebner et al., 2013; Miyata et al., 1999; Rinaldi et al., 2013).



295

296 **Figure 5. Co-expressed Late target genes are expressed in developing granule cells or Purkinje cells with**
 297 **common roles in cerebellar development.** A) Line plot and heatmap showing mean z-score expression throughout
 298 the cerebellar time course. B) Line plot representation of expression pattern throughout time for each cluster. C)
 299 Known cerebellar genes in each cluster and *in situ* hybridization showing spatial expression at peak expression ages.
 300 ISH images were taken from the Developing Mouse Atlas provided by the Allen Brain Atlas conducted at P4.5 for
 301 all clusters. D) Gene Ontology (GO) enrichment analysis of all target genes of Late active enhancers, displaying the
 302 top enriched GO terms. Size of the dots indicates the number target genes within a given GO term and the gene ratio
 303 (x-axis) is equal to the number of genes within the GO category divided by the total number of genes in the cluster.
 304 Color scale indicates the adjusted p-value for each GO term.

305 A GO enrichment analysis was conducted for each Cluster; with no significantly
 306 enriched Cluster-specific GO terms. However, if all Late enhancer target genes were combined,
 307 several enriched GO terms emerged including ones involved in postnatal neuronal development,

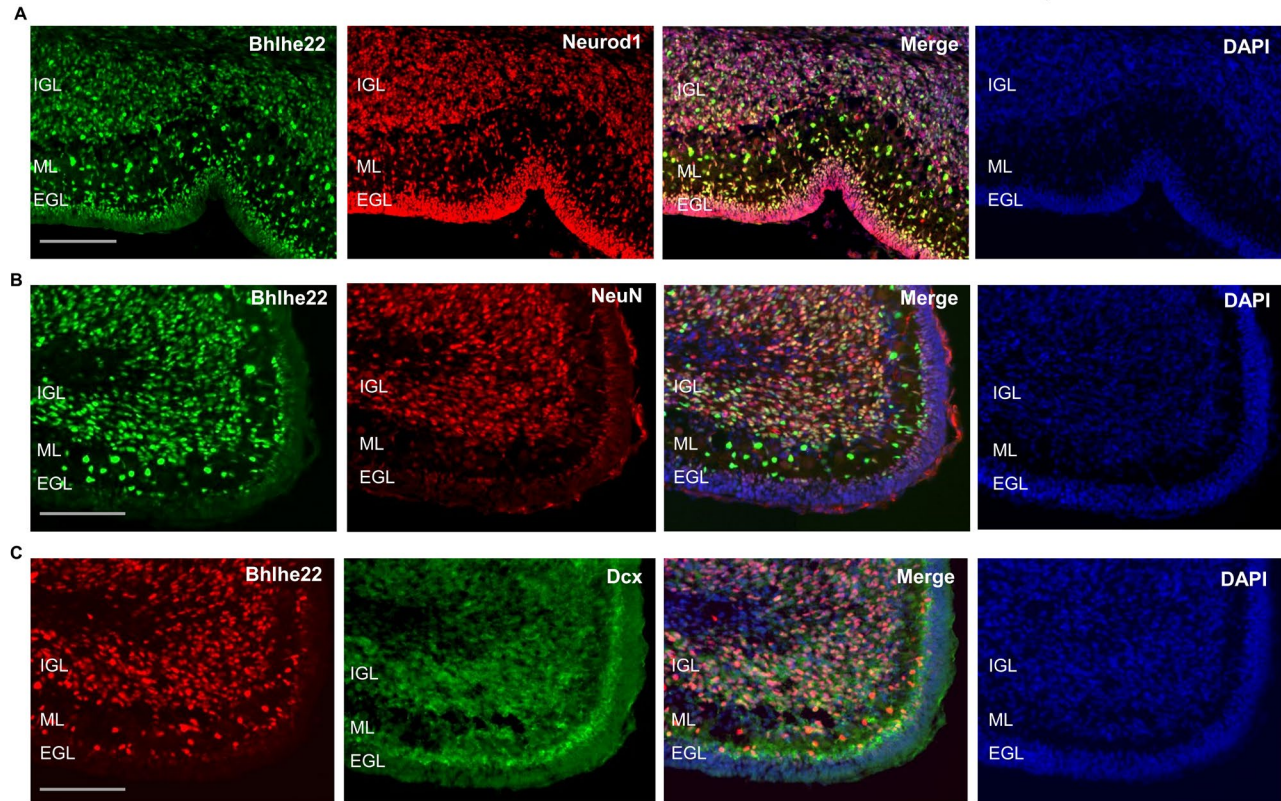
308 such as **neuron death** (GO:0070997, p-value: 0.003), **neurotransmitter transport**
309 (GO:0006836, p-value: 0.006) and **regulation of synaptic vesicle exocytosis** (GO:2000300, p-
310 value: 0.005) (**Figure 5D**). Overall, this analysis provides a working framework for the
311 placement of hundreds of genes into the overall structure of embryonic or postnatal cerebellar
312 development

313

314 ***Bhlhe22* is a novel regulator of granule cell development**

315 To demonstrate the utility of our results, we sought to identify target genes not
316 previously identified in cerebellar development. We focused on Late Cluster 1, which contained
317 target genes expressed in granule cells. We hypothesized that genes within this cluster regulated
318 postnatal granule cell differentiation. To identify genes in this cluster regulating granule cell
319 development, we filtered these genes relative to their interaction with *Atoh1*, the lineage defining
320 molecule for granule cells and other glutamatergic neurons in the developing cerebellum (Ben-
321 Arie et al., 1997). The genes were filtered using the following criteria: 1) *Atoh1* is bound to the
322 predicted enhancer during postnatal development (Klisch et al., 2011) and 2) the genes are
323 differentially expressed in the *Atoh1*-null mouse (Klisch et al., 2011). Among the top 15 genes in
324 the filtered list, we identified **4** novel genes and **11** genes that have previously been implicated in
325 postnatal granule cell development (Supplementary Table 1). The known genes provided
326 validation for our approach. The novel genes included *Bhlhe22* (also known as *Bhlhb5*), *Purb*,
327 *Klf13* and *Sox18*. We focused particularly on *Bhlhe22* as it has previously been implicated in the
328 differentiation of neurons in the cortex (Joshi et al., 2008). An enhancer ~2 kb upstream of the
329 *Bhlhe22* transcriptional start site was identified and is bound by *Atoh1* during postnatal
330 development (**Supplemental Figure 3A**). This enhancer displayed H3K27ac activity highly
331 correlated (Pearson correlation coefficient = 0.98) to *Bhlhe22* expression, which consistently
332 rises throughout cerebellar development and peaks at P9.5 (**Supplemental Figure 3B**).

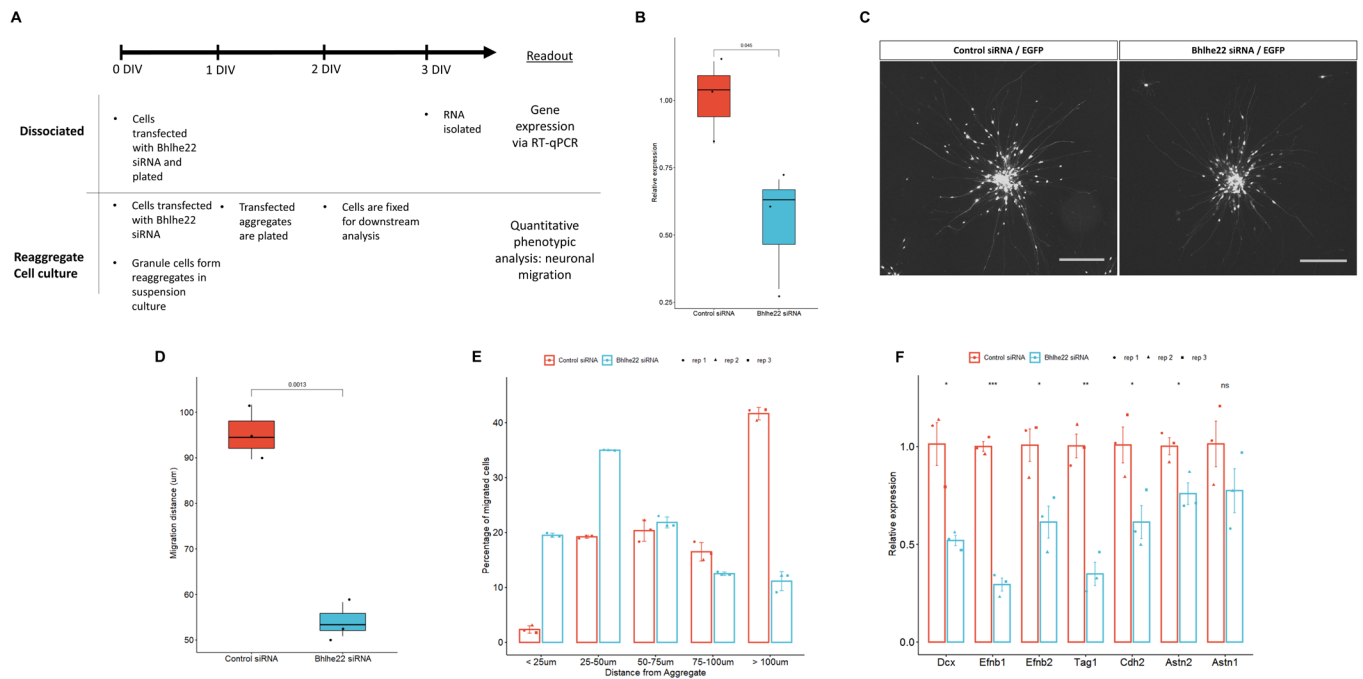
333 To attain a cellular resolution of the expression pattern for *Bhlhe22* over developmental
334 time, a time-course of protein expression using immunofluorescent staining spanning cerebellar
335 development was conducted. *Bhlhe22* expression was observed in cells within the inner external



336
337 **Figure 6. Bhlhe22 is expressed in differentiating granule cells in postnatal cerebellar development.** A) Bhlhe22
338 (green) and Neurod1 (red) immunofluorescent co-staining at P9.5 of taken from a posterior lobe IX. B) Bhlhe22
339 (green) and NeuN (red) immunofluorescence co-staining at P6 taken from posterior lobe IX. C) Bhlhe22 (red) and
340 Dcx (green) immunofluorescent co-staining at P6 showing the posterior lobe IX; Labels: EGL= external granular
341 layer IGL = inner granular layer, ML = molecular layer, Scalebars = 100um.

342
343 granule layer (EGL), molecular layer and in the inner granule layer (IGL) of the postnatal
344 cerebellum (**Figure 6A**). To identify whether Bhlhe22 is expressed in differentiating granule
345 cells, co-staining experiments were performed with Neurod1 and NeuN which mark
346 differentiating and mature granule cells, respectively (Miyata et al., 1999; Weyer & Schilling, 2003).
347 At P6.5, colocalization between Bhlhe22 and Neurod1 was observed, indicating expression in
348 differentiating and migrating granule cells (**Figure 6A**). Co-staining between Bhlhe22 and NeuN
349 expression was also observed, indicating expression in maturing granule cells found within the
350 IGL (**Figure 6B**). To confirm whether the Bhlhe22-positive cells within the molecular layer were
351 migrating granule cells, we performed a double labelling experiment for a neuronal migration
352 marker Doublecortin (Takács, Zaninetti, Vig, Vastagh, & Hámori, 2008). Colocalization between
353 Doublecortin and Bhlhe22 was observed in cells within the inner EGL and the molecular layer,
354 confirming Bhlhe22 expression in migrating granule cells (**Figure 6C**).

355 We then investigated the role that Bhlhe22 plays in postnatal granule cell development
 356 using a well-established *in vitro* system (Lee, Greene, Mason, & Manzini, 2009). Three sets of
 357 experiments were performed using isolated granule cells from P6.5 cerebella transfected with
 358 siRNA targeting Bhlhe22 transcripts (**Figure 7A**). First, to determine if Bhlhe22 expression was
 359 diminished, changes in gene expression were assessed after 3 days *in vitro* (DIV) using reverse
 360 transcriptase quantitative PCR (RT-qPCR). A 50% reduction of Bhlhe22 expression, on average,
 361 was found in treated cultures compared to controls (**Figure 7B**).



362
 363 **Figure 7. Knockdown of Bhlhe22 reduces migration of cultured cerebellar granule cells.** **A)** Workflow for
 364 dissociated and reaggregate postnatal granule cell cultures. **B)** RT-qPCR analysis of Bhlhe22 gene expression in
 365 dissociated postnatal granule cell cultures after treatment with Bhlhe22 siRNA. Gene expression was normalized
 366 relative to the expression of the co-transfected EGFP protein to account for transfection variability between cultures.
 367 Data are presented as mean \pm SD (n = 3). **C)** Image of cultured cerebellar granule cell reagggregates treated with
 368 control and Bhlhe22 siRNA. Shown are EGFP positive cells indicating successful transfection. Scalebars = 100µm.
 369 **D)** Box plot displaying mean distance of granule cell migration from the aggregate. Value above indicates a
 370 statistical difference between control cultures and those treated with Bhlhe22 siRNA (p-value = 0.0013). **E)** Bar plot
 371 showing the percentage of cells migrated at different distances from the aggregate for control and Bhlhe22 siRNA
 372 treated cerebellar granule cell cultures. **F)** RT-qPCR analysis of gene expression of cell adhesion molecules in
 373 dissociated postnatal granule cell cultures after treatment with Bhlhe22 siRNA. Gene expression was normalized
 374 relative to the expression of the co-transfected EGFP protein to account for transfection variability between cultures.
 375 Data are presented as mean \pm SD (n = 3). Symbols: *: p \leq 0.05, **: p \leq 0.01, ***: p \leq 0.001, which indicate
 376 statistical differences observed between Bhlhe22 siRNA treated samples and controls. All error bars represent the
 377 standard error of the man
 378

379 Second, phenotypes of the transfected cells were examined; examining their neuritic
380 outgrowths from the aggregate, and the migration of granule cells from the aggregates, within the
381 first 24 hours of plating (Gartner, Collin, & Lalli, 2006). Neuritic outgrowth was unaffected,
382 however there was a marked reduction in migration (**Figure 7C**). Bhlhe22 siRNA transfected
383 cells travelled on average 54.2um from the edge of the aggregate, a 50% reduction compared to
384 control samples (**Figure 7D**). Examining the distribution of migrated cells from the edge of the
385 aggregate, there was a higher percentage of Bhlhe22 siRNA transfected granule cells migrating
386 less than 50um, while the majority of the cells in control samples migrated 100um and beyond
387 (**Figure 7E**).

388 Third, changes in the expression of cell adhesion molecules that are known to be
389 involved in granule cell development were assessed (Consalez et al., 2021; Wang et al., 2007). A
390 significant reduction of *Efnb1*, *Efnb2*, *Tag1*, *Cdh2* and *Astn2* was observed in Bhlhe22
391 knockdown granule cell cultures compared to controls (**Figure 7F**). In addition to these genes,
392 we also found a significant reduction in Doublecortin (*Dcx*) expression. Taken together, these *in*
393 *vitro* knockdown experiments reveal a novel function for Bhlhe22, a gene that was identified by
394 our temporal enhancer-target gene analysis and was predicted to have a critical role in postnatal
395 granule cell development.

396

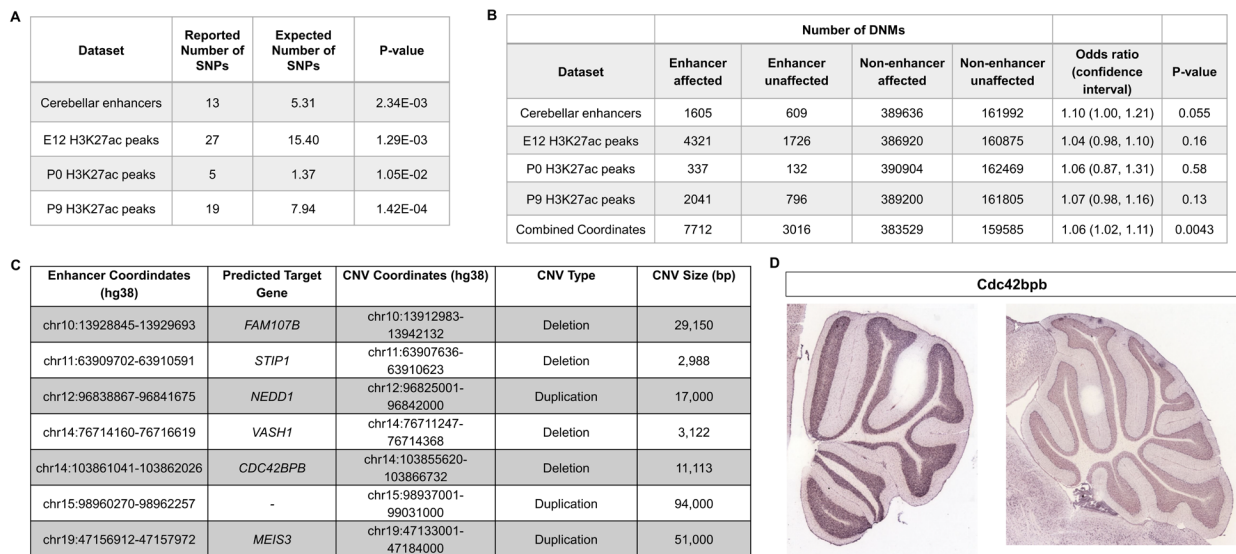
397 **Active cerebellar enhancers are enriched for common and *de novo* genetic variants** 398 **associated with autism spectrum disorder.**

399 Genome wide association studies (GWAS) have revealed that the majority of variants
400 associated with neurodevelopmental diseases are found within non-coding regulatory sequences,
401 particularly enhancers (Visel, Rubin, & Pennacchio, 2009). Given the emerging importance of the
402 cerebellum in the etiology of autism spectrum disorder (ASD), we tested whether ASD-
403 associated variants are enriched in cerebellar enhancers. The software tool GREGOR (Genomic
404 Regulatory Elements and Gwas Overlap algoRithm) was used to evaluate the enrichment of
405 common genetic variants associated with ASD in cerebellar enhancers (Schmidt et al., 2015). ASD
406 associated SNPs were retrieved from the GWAS Catalog (Buniello et al., 2019) and a stringent
407 filter was applied to identify SNPs associated with the ASD (Supplementary Table 2). We
408 examined 174 ASD-associated SNPs with a maximum p-value of 9E-06 (Buniello et al., 2019).
409 ASD-associated SNPs were enriched in cerebellar enhancers (p-value = 2.34E-03) and in

410 H3K27ac peaks at E12, P0, and P9 (p-values of 1.29E-03, 1.05E-02 and 1.42E-04, respectively)
 411 (**Figure 8A**). For the 13 cerebellar enhancers containing ASD-associated SNPs, we identified 12
 412 predicted target genes (Supplementary Table 3). Among these, three (*PAX6*, *TCF4*, and *ZMIZ1*)
 413 are ASD risk genes according to the Simons Foundation Autism Research Initiative (SFARI)
 414 gene database (Banerjee-Basu & Packer, 2010).

415 *De novo* mutations (DNMs) (variants present in the genome of a child but not his or her
 416 parents) have been found to play a significant role in the etiology of ASD, including those found
 417 in non-coding regions of the genome (Grove et al., 2019; Yuen et al., 2016). We hypothesized that
 418 DNMs within cerebellar enhancers would be more prevalent in ASD-affected individuals
 419 compared with their unaffected siblings. We used whole-genome sequencing data from 2,603
 420 ASD-affected individuals and 164 unaffected siblings from the MSSNG cohort (C Yuen et al.,
 421 2017), as well as 2,340 ASD-affected individuals and 1,898 unaffected siblings from the Simons
 422 Simplex Collection (SSC) (Fischbach & Lord, 2010) to analyze the prevalence of DNMs in ASD-
 423 affected individuals compared with their unaffected siblings.

424



425

426

427 **Figure 8. Cerebellar enhancers are enriched for GWAS SNPs and DNMs associated with ASD.** **A)** Number of
 428 ASD-associated GWAS variants identified in cerebellar enhancers and H3K27ac peaks called from E12, P0, and P9
 429 samples. **B)** Enrichment of *de novo* single nucleotide variants and indels in ASD-affected individuals compared with
 430 their unaffected siblings. Counts are not equal to the sum of the four enhancer types because some enhancers are
 431 categorized as more than one type. **C)** Gene targets for enhancers overlapped by *de novo* CNVs in the SSC cohort.
 432 **D)** *In situ* hybridization showing *Cdc42bpb* expression in the lateral (left) and medial (right) adult mouse cerebellum
 433 (REF mouse brain atlas). Note expression is found in granule cells, particularly those of the lateral cerebellum.

434

435 We found that DNMs (specifically *de novo* single nucleotide variants and indels) in
436 cerebellar enhancers and H3K27ac peaks from E12, P0 and P9 were enriched in ASD-affected
437 individuals, with odds ratios ranging from 1.04 to 1.10 (**Figure 8B**). While these differences
438 were not statistically significant for cerebellar enhancers and peak coordinates individually,
439 statistical significance was achieved when combined (odds ratio=1.06; p-value=0.0043). We also
440 identified *de novo* CNVs overlapping cerebellar enhancers. Since the number of such CNVs was
441 too small to perform statistical enrichment tests, we selected a subset of 7 of these CNVs (4
442 deletions and 3 duplications) for further characterization to identify candidates for association
443 with ASD (**Figure 8C**). The most promising candidate was an ~11 kb deletion overlapping an
444 enhancer predicted to target *CDC42BPB*, which has previously been implicated in
445 neurodevelopmental phenotypes (Chilton et al., 2020). By visual validation in Integrative
446 Genomics Viewer (Robinson et al., 2011), we verified that this deletion was truly *de novo*
447 (Supplementary Figure 4). *CDC42BPB* is expressed in the granule cell layer of the adult mouse
448 cerebellum (**Figure 8D**) and is expressed in the lateral aspects of the cerebellum but not the
449 medial cerebellum.

450

451 **Discussion**

452 The current model of gene expression regulation during brain development posits that
453 temporal and spatial transcription is under the intricate control of thousands of non-coding
454 enhancer sequences (Nord & West, 2020). This model has emerged from the findings of several
455 studies of enhancer activity in various parts of the developing brain (Nord et al., 2013; Pattabiraman
456 et al., 2014; Visel et al., 2013). In our study on the cerebellum, we performed an assessment of
457 enhancer activity through genome-wide profiling of H3K4me1 and H3K27ac deposition at three
458 time points during embryonic and early postnatal times. These datasets were utilized to define
459 functional enhancer elements with temporally specific activity during these developmental ages.
460 In doing so, we establish the first catalog of predicted enhancers active during embryonic
461 cerebellum development. Through a motif enrichment analysis, neural TF motifs were found to
462 be enriched in cerebellar enhancers which may drive temporally specific enhancer activation.
463 This analysis highlighted a novel regulatory role for several understudied TFs in the context of
464 cerebellar development. These data were then integrated with a transcriptomic time course to
465 identify predicted target genes to inform our understanding of enhancer regulation in the

466 developing cerebellum. Through unbiased clustering, we identified enhancer-regulated co-
467 expression gene programs with spatially distinct patterns of expression and unique biological
468 functions during embryonic and postnatal development. Further analysis of these results led to
469 the discovery of novel cell-type marker and regulator of cerebellar development and highlights
470 the importance of enhancer regulation during brain development and the etiology of ASD.

471

472 **Cerebellar enhancers regulate gene expression important for distinct stages of neuronal** 473 **development**

474 Identification of enriched TF binding sites and putative target genes indicated that
475 cerebellar enhancers likely play a regulatory role in various phases of neuronal development. In
476 agreement with our results, previous examinations of active non-coding regulatory sequences
477 revealed that neural progenitor cells and mature neurons exhibit distinct signatures of enhancer-
478 associated histone profiles, DNA methylation, chromatin conformation and enhancer-promoter
479 interactions (Bonev et al., 2017; de la Torre-Ubieta et al., 2018; Lister et al., 2013; Whyte et al., 2012).
480 Bonev et al. (2017) examined changes in enhancer-promoter interactions between transgenic cell
481 lines FACS sorted for embryonic stem cells, neural progenitors and mature neurons and
482 identified that changes in enhancer-promoter contacts are cell-state specific and correlate with
483 changes in gene expression (Bonev et al., 2017). When comparing contacts in neuro-progenitors
484 and mature neurons, a decrease in the interaction strength was observed between active domains
485 compared to an increased strength in inactive domains, indicating a shift in usage of regulatory
486 sequences. These changes were also reflected at the level of TF binding, as interactions at Pax6-
487 bound sites, a TF marking neural progenitors, were stronger in neural progenitors than in
488 neurons, while NeuroD2-bound sites, a TF marking mature neurons, were stronger in neurons
489 than NPCs (Bonev et al., 2017). This shift in enhancer usage throughout cortical development is
490 also reflected in DNA methylation profiles, where fetal enhancers are hypermethylated and
491 decommissioned in the adult brain, while enhancers regulating adult gene expression were
492 hypomethylated (Lister et al., 2013). Hypermethylation was accompanied by a decrease in
493 H3K4me1, H3K27ac and DNase hypersensitivity while the increase was observed after
494 hypomethylation (Lister et al., 2013). Our study supports the importance of temporally-specific

495 activity during different stages of neuron development *in vivo* and details the processes driven by
496 enhancer-regulated expression during embryonic and early postnatal brain development.

497 Expression analysis of two genes novel to cerebellar development, Pax3 and Bhlhe22,
498 supported the notion that enhancer profiles are specific to developmental stage. TF enrichment
499 analysis identified Pax3 preferentially enriched in Early active enhancers and robust expression
500 of Pax3 was localized to GABAergic interneuron progenitor cells. Interestingly, through further
501 examination of cerebellar single-cell RNA-seq data produced by Carter et al. (2018), we found
502 that Pax3 expression is enriched in GABAergic progenitors and differentiating GABAergic
503 interneurons (Carter et al., 2018). Analysis of predicted gene targets of Late active enhancers
504 identified Bhlhe22 as a novel gene expressed in postnatal differentiated granule cells, and *in*
505 *vitro* knockdown experiments in primary granule cells indicated Bhlhe22 regulates granule cell
506 migration potentially through regulation of cell adhesion molecule expression. These results are
507 supported by findings in the developing cortex, where Bhlhe22 has been shown to regulate post-
508 mitotic acquisition of area identity in layers II-V of the somatosensory and caudal motor cortices
509 (Joshi et al., 2008). The contrasting expression profiles of Pax3 and Bhlhe22 highlight the wide-
510 ranging developmental impact of enhancer-mediated gene expression regulation.

511 Our findings from the TF enrichment and gene target analyses generated from
512 preferentially active postnatal enhancers indicate that many of the enhancers captured are active
513 in the developing granule cells and Purkinje cells. We attribute this apparent bias to our whole
514 tissue approach, as granule cells and Purkinje cells are the predominant cells in the cerebellum at
515 that time, making it more likely to capture signals specific to these cells compared to other less
516 abundant cell types. Our study therefore reveals that to elucidate enhancers specifically active
517 within less abundant cell types, a more granular approach may be required through single-cell
518 examination of chromatin accessibility, such as single cell ATAC-seq. This approach can be
519 coupled with the abundance of scRNA-seq data that has been collected in the developing
520 cerebellum. This strategy has seen success in the developing cortex and more recently in the
521 cerebellum (Preissl et al., 2018; Sarropoulos et al., 2021).

522

523

524 **Co-expressed gene targets of cerebellar enhancers display cell type-specific expression**
525 **patterns**

526 In addition to being temporally-specific, recent evidence indicates that enhancer activity
527 is cell type specific in the brain (Blankvoort, Witter, Noonan, Cotney, & Kentros, 2018). This is
528 highlighted in the identification of cerebellar enhancer target gene clusters for Early and Late
529 active enhancers with cell specific patterns of expression (Figure 4 and 5). For example, distinct
530 boundaries can be seen in gene expression from Early Clusters 3 and 4 at E11.5 between cells in
531 the subpial stream (Cluster 4) and neuroepithelium (Cluster 3) where neural precursors of two
532 separate lineages, the glutamatergic cerebellar nuclei and GABAergic cerebellar nuclei and
533 Purkinje cells, are found, respectively. These sharp borders are reminiscent of the small domains
534 of distinct enhancer activity identified in neural progenitors in the telencephalon, which were
535 found to fate-map to specific prefrontal cortex subdivisions (Pattabiraman et al., 2014). We see a
536 similar pattern in the more developed postnatal cerebellum, observing a spatial distinction
537 between Late Clusters 1/3 and 2/4 delineating expression in granule cells and Purkinje cells,
538 respectively. This cell type specific enhancer usage is demonstrated in the adult brain.
539 Blankvoort et al (2018) (Blankvoort et al., 2018) used ChIP-seq analysis of microdissected
540 subregions of the adult mouse cortex to reveal unique enhancer profiles pertaining to each
541 region. Additionally, Nott et al (2019) (Nott et al., 2019) identified enhancer-promoter interactome
542 maps specific to the major cell types in the cortex, which included neurons, microglia,
543 oligodendrocyte and astrocytes. Enriched GO terms for each cerebellar target gene clusters were
544 cell-type and temporally specific, highlighting enhancer specificity. Functionally annotating their
545 respective clusters provides a working hypothesis for hundreds of genes, which can be used as a
546 jumping point for future in-depth studies in the cerebellum. Collectively, these findings support
547 the notion that the cell types in the cerebellum have specific enhancer signatures relevant which
548 are reflected by the expression and functions of their target genes.

549

550 **GWAS SNPs and DNMs associated with ASD are enriched in cerebellar enhancers**

551 Having established and characterized enhancer sequences in the cerebellum, we sought to
552 elucidate the potential involvement of these regions in the etiology of neurological disorders;
553 imaging and quantitative data show consistent cerebellar abnormalities, particularly in cases of

554 individuals with autism (Limperopoulos et al., 2014) (Stoodley & Limperopoulos, 2016). Our results
555 indicate that cerebellar enhancer sequences are significantly enriched for GWAS variants and
556 DNMs associated with ASD, suggesting an important role for enhancers in contributing to the
557 condition. PAX6 was among 12 target genes of cerebellar enhancers containing ASD-associated
558 variants and is classified in the SFARI as a ASD risk gene. The deletion of Pax6 in the murine
559 cerebellum results in aberrant development of the glutamatergic cells in the cerebellum: the
560 cerebellar nuclei, unipolar brush cells and granule cells (Yeung et al., 2016). Behavioral analysis
561 of Pax6 animal models has also indicated a possible link between this gene and autistic-like
562 behavior (Umeda et al., 2010). Additionally, Pax6 has been linked with WAGR (Wilm's tumor,
563 Aniridia, Genitourinary malformations, and mental Retardation syndrome) which is co-morbid
564 for ASD. Our analysis invites future investigation these target genes and how perturbation of
565 their expression may lead to ASD phenotypes.

566 Of the target genes of the enhancers that overlapped *de novo* CNVs in the SSC cohort,
567 none have been previously associated with cerebellar development. Interestingly, one of these
568 target genes, *CDC42BPB*, has recently been associated with neurodevelopmental disorders
569 including ASD (Chilton et al., 2020). This gene is a serine/threonine protein kinase and codes for
570 MRCK β (myotonic dystrophy-related Cdc42-binding kinase beta), a regulator of cell
571 cytoskeletal reorganization and cell migration (Pichaud, Walther, & Nunes de Almeida, 2019). Of
572 note, the CNV associated with this gene deletes the entire enhancer. *CDC42BPB* shows
573 expression in the granule cell layer of the lateral adult cerebellum, which has been associated
574 with cognitive functions (Koziol et al., 2014).

575 Together, our data serves as an invaluable resource for future studies, by providing
576 candidate genes involved in cerebellar development with potentially meaningful impact in the
577 etiology of ASD and other neurodevelopmental disabilities.

578

579 **Materials and Methods**

580 **Mouse strains and husbandry**

581 C57BL/6 J mice were originally purchased from JAX laboratory and maintained and bred in a
582 pathogen-free animal facility with 12/12 hour light/dark cycle and a controlled environment.
583 Embryonic ages utilized in these experiments were confirmed based upon the appearance of a

584 vaginal plug. The morning that a vaginal plug was detected was designated as E0.5. Pregnant
585 females were cervically dislocated and embryos were harvested from the uterus. Postnatal ages
586 were determined based upon the date of birth with the morning of the observation of newborn
587 pups considered as P0.5. All studies were conducted according to the protocols approved by the
588 Institutional Animal Care and Use Committee and the Canadian Council on Animal Care at the
589 University of British Columbia.

590

591 **Tissue preparation for chromatin immunoprecipitation**

592 C57BL/6 J mice (male and female) at E12.5, P0.5 and P9.5 (henceforth referred to as E12, P0,
593 and P9) were decapitated for dissection of cerebella. Cerebella were dissected and collected in
594 ice cold Dulbecco's PBS (DPBS) without magnesium or calcium and subsequently washed 2x
595 for 5 minutes. Samples from each litter were pooled and trypsinized in DPBS containing 0.25%
596 trypsin for 10, 15 and 30 min at room temperature for E12, P0 and P9, respectively. Following 3
597 washes with fresh DPBS, the tissue was triturated with 3 progressively smaller (1, 0.5, 0.1mm)
598 bore polished and sterile pipettes in DPBS containing 250U/ml DNase, 0.25% glucose, and
599 8mg/ml BSA. The triturated cells were diluted 1:4 with cold DPBS and passed through a cell
600 strainer (40µm mesh) to remove large cellular debris. The cells were collected by mild
601 centrifugation, washed in fresh DPBS and counted. The cells were split into 100,000 cell
602 aliquots, pelleted and snap frozen using liquid nitrogen. Cell pellets were stored at -80°C.

603

604 **Histone chromatin immunoprecipitation**

605 We performed native chromatin immunoprecipitation (ChIP) using validated antibodies against
606 H3K4me1 and H3K27ac according to previously established protocols by the International
607 Human Epigenomics Consortium (IHEC) (Lorzadeh, Lopez Gutierrez, Jackson, Moksa, & Hirst,
608 2017). Briefly, cells were lysed in mild non-ionic detergents (0.1% Triton X-100 and
609 Deoxycholate) and protease inhibitor cocktail (Calbiochem) to preserve the integrity of histones
610 harbouring epitopes of interest during cell lysis. Cells were digested by Micrococcal nuclease
611 (MNase) at room temperature for 5 minutes and 0.25mM EDTA was used to stop the reaction.
612 Antibodies to H3K4me1 (Diagenode: Catalogue #C15410037, lot A1657D) and H3K27ac
613 (Hiroshi Kimura, Cell Biology Unit, Tokyo Institute of Technology) were incubated with anti-
614 IgA magnetic beads (Dynabeads from Invitrogen) for 2 hours. Digested chromatin was incubated

615 with magnetic beads alone for 1.5 hours. Digested chromatin was separated from the beads and
616 incubated with antibody-bead complex overnight in immunoprecipitation buffer (20mM Tris-
617 HCl pH 7.5, 2mM EDTA, 150mM NaCl, 0.1% Triton X-100, 0.1% Deoxycholate). The resulting
618 immunoprecipitations were washed 2 times by low salt (20mM Tris-HCl pH 8.0, 2mM EDTA,
619 150mM NaCl, 1% Triton X-100, 0.1% SDS) and then high salt (20mM Tris-HCl pH 8.0, 2mM
620 EDTA, 500 mM NaCl, 1% Triton X-100, 0.1% SDS) wash buffers. Immunoprecipitations were
621 eluted in an elution buffer (1% SDS, 100 mM Sodium Bicarbonate) for 1.5 hours at 65°C.
622 Remaining histones were digested by Protease (Invitrogen) for 30 minutes at 50°C and DNA
623 fragments were purified using Ampure XP beads (Beckman Coulter). The library preparation
624 was conducted by Diagenode ChIP-seq/ChIP-qPCR Profiling service (Diagenode Cat#
625 G02010000) using the MicroPlex Library Preparation Kit v2 (Diagenode Cat. C05010013). 50-
626 bp single-end sequencing was performed on all libraries by Diagenode (Belgium) on an Illumina
627 HiSeq 3000 platform. Two independent biological replicates were performed for each antibody
628 and developmental time point.

629

630 **Histone modification ChIP-seq data processing**

631 The sequencing data were uploaded to the Galaxy web platform (usegalaxy.org) for analyses
632 (Afgan et al., 2016). 50-bp single-end ChIP-seq reads were aligned to the NCBI37/mm9 reference
633 genome and converted to binary alignment/map (BAM) format by Bowtie2 v.2.3.4 (Langmead,
634 Trapnell, Pop, & Salzberg, 2009) with default parameters. Duplicate reads were marked using
635 Picard v.1.52. Peak enrichment was computed using MACS v.2.1.1 (Zhang, Y. et al., 2008) with a
636 false discovery rate (FDR) cutoff of 0.01 (p-value < 1E-5) using input samples as a control for
637 each replicate. bigWigs were generated and normalized by the total number of mapped reads
638 using the BamCompare and profiles were generated from these bigWigs by calculating average
639 coverage in 50 bp bins using Deeptools v.3.3 (Ramírez et al., 2016) for downstream analysis and
640 visualization.

641

642 **Identification of active cerebellar enhancers**

643 We first determined consensus peaks between replicates for both H3K27ac and H3K4me1 peaks
644 collected at E12, P0 and P9 using the *intersect* function from Bedtools v.2.28 (Quinlan & Hall,
645 2010). Robust active cerebellar enhancers were identified by overlapping replicated H3K27ac

646 and H3K4me1 peaks called for E12, P0 and P9 samples. The genomic coordinates of the
647 H3K27ac peaks that overlapped with H3K4me1 enriched regions at the same age were used for
648 our list of robust active cerebellar enhancers. We then removed peaks found within promoter
649 sequences by eliminating any peaks found 500bp upstream or downstream of transcription start
650 sites (TSSs) in the developing cerebellum as determined previously (Zhang et al., 2018). The
651 resulting list of robust active cerebellar enhancer sequences at E12, P0, and P9 were used for
652 downstream analysis.

653 For the comparative analysis with cerebellar postnatal enhancers previously published by Frank
654 et al. (2015), H3K27ac and DNase-seq peak coordinates were downloaded from Gene
655 Expression Omnibus (GEO) (GSE60731). The following sequences were downloaded from
656 public enhancer databases: 1) enhancers downloaded from the VISTA Enhancer Browser
657 (<https://enhancer.lbl.gov/>) (Visel et al., 2007) with hindbrain activity were filtered using the
658 ‘Advanced Search’ tool, selecting “hindbrain” under Expression Pattern and retrieving only
659 mouse sequences with positive signal and 2) mouse cerebellar neonate enhancer coordinates
660 were downloaded from the Enhancer Atlas 2.0 repository
661 (<http://www.enhanceratlas.org/downloadv2.php>) (Gao & Qian, 2020). For the comparisons,
662 sequences were overlapped with our robust cerebellar enhancer peaks and H3K27ac peaks at
663 E12, P0 and P9 using Bedtools v.2.28(Quinlan & Hall, 2010).

664

665 **Differential binding analysis**

666 Aligned read counts (BAM file format) from our H3K27ac ChIP-seq experiments mapped to our
667 robust active cerebellar enhancers for E12, P0 and P9 samples were used as input to the package
668 DiffBind v1.4.2 (Stark & Brown, 2011). Read counting at each genomic location was conducted,
669 which was subsequently normalized by experimental input samples. The result of counting is a
670 binding affinity matrix containing normalized read counts for every sample at each robust active
671 cerebellar enhancer. For differential binding affinity analysis, three contrasts were set up in
672 DiffBind: E12 vs P0, E12 vs P9, and P0 vs P9. Differential binding was determined by DiffBind
673 using a negative binomial test at an FDR < 0.05 threshold. The FDRs and normalized signal
674 difference for each contrast were plotted using the EnhancedVolcano package in R (Kevin Blighe,
675 Sharmila Rana, & Myles Lewis, 2020).

676

677 **Temporal classification of cerebellar enhancers**

678 To determine cerebellar enhancers with embryonic-specific activity, H3K27ac signal at E12 was
679 compared to P0 and P9. Enhancers with significantly higher signal at E12 for either contrast
680 were considered “Early” active enhancers. A region found to be enriched for both contrasts was
681 counted as one enhancer. To determine cerebellar enhancers with postnatal-specific activity,
682 H3K27ac signal at P9 was compared to E12 and P0. Enhancers with significantly higher signal at
683 P9 for either contrast were considered “Late” active enhancers. A region found to be enriched for
684 both contrasts was counted as one enhancer. To determine cerebellar enhancers with activity
685 specific to birth, H3K27ac signal at P0 was compared to P9 and E12. Enhancers with
686 significantly higher signal at P0 in both contrasts would identify enhancers that peaked in
687 activity at P0. We did not identify any enhancers that peaked in activity at P0 and conducted the
688 remaining analysis for only Early and Late enhancers.

689

690 **Transcription factor motif enrichment analysis**

691 Transcription factor motif enrichment was calculated using the software HOMER using the
692 script FindMotifsGenome.pl with default parameters (Heinz et al., 2010). Analyses for Early and
693 Late active enhancers were conducted separately. Motif enrichment was statistically analyzed
694 using a cumulative binomial distribution. Enriched motifs were aligned with known transcription
695 factor binding sites to determine the best matches. Top known motif matches were filtered based
696 on expression within the developing cerebellum at E12 for “Early” active enhancers and P9 for
697 “Late” active enhancers.

698

699 **Cerebellar enhancer target gene prediction and co-expression analysis**

700 To identify possible gene targets of our robust cerebellar enhancers, the correlation between
701 H3K27ac signal and mRNA expression of genes located in *cis* at E12, P0 and P9 was calculated.
702 For a given enhancer, a gene located in *cis* was considered a possible target if it was positively
703 correlated with H3K27ac signal throughout time. These genes were then filtered based on
704 location using conserved topologically associating domains (TADs), which are areas of the
705 genome that preferentially interact (Dixon et al., 2012). These TADs are conserved between
706 different cell types and even across species and were established using Hi-C data generated,
707 previously. Gene target candidates for a given enhancer were curated for those located within the

708 same TAD. Predicted gene targets were then ranked based on their Pearson correlation
709 coefficient value. For the predicted gene targets of Early and Late active enhancers, we
710 conducted *k-means* clustering of predicted gene targets separately. Input for this analysis was
711 gene expression captured from cerebella at 12 embryonic and postnatal time points (Zhang et al.,
712 2018). Briefly, gene expression was quantified using Cap Analysis of Gene Expression followed
713 by sequencing (CAGE-seq) for mouse cerebellar samples dissected every 24 hours from E11-P0
714 and then every 72 hours until P9 (12 in vivo time points in total). The number of clusters for the
715 *k-means* clustering was determined using the Elbow analysis for each classified group of
716 enhancers: Early (n=4) and Late (n=4).

717

718 **Tissue preparation for histology**

719 Embryos harvested between E11.5 to E15.5 were fixed by immersion in 4% paraformaldehyde in
720 0.1M phosphate buffer (PB, pH 7.4) for 1 hour at 4°C. Postnatal mice between P0.5 to P6.5 were
721 perfused through the heart with a saline solution followed by 4% paraformaldehyde/0.1M PBS.
722 The brain tissues were isolated and further fixed in 4% paraformaldehyde in 0.1M PB for 1 hour
723 at room temperature. Fixed tissues were rinsed with PBS, followed by cryoprotection with 30%
724 sucrose/PBS overnight at 4°C before embedding in the Optimal Cutting Temperature compound
725 (Tissue-Tek). Tissues were sectioned at 12um for immunofluorescence experiments and
726 cryosections were mounted on Superfrost slides (Thermo Fisher Scientific), air dried at room
727 temperature, and stored at -80°C until used. Sagittal sections were cut from one side of the
728 cerebellum to the other (left to right, or vice versa). In all cases, observations were based on a
729 minimum of 3 embryos per genotype per experiment.

730

731 **Cerebellar immunostaining**

732 Tissue sections were first rehydrated in PBS (3 x 5 minute washes) followed by a phosphate
733 buffered saline with Triton X-100 (PBS-T) rinse. Sections were then incubated at room
734 temperature for 1 hour with blocking solution (0.3% BSA, 10% normal goat serum, 0.02%
735 sodium azide in PBS-T). Following the blocking step, the slides were incubated with primary
736 antibody in incubation buffer (0.3% BSA, 5% normal goat serum, 0.02% sodium azide in PBS-
737 T) at room temperature overnight in a humid chamber. Following the overnight incubation, the
738 slides were rinsed in 3 x 10 minute PBS-T washes. The sections were then incubated with the

739 appropriate secondary antibody at room temperature for 1 hour, followed by three 0.1M PB
740 washes and one 0.01M PB wash. Coverslips were applied to the slides using FluorSave mounting
741 medium (345789, Calbiochem). The primary antibodies used were: rabbit anti-Bhlhe22 (1:1000,
742 a gift from Dr. Michael Greenburg, Harvard University), mouse anti-Neurod1 (1:500, Abcam,
743 ab60704), mouse anti-Pax3 (1:500, R&D systems, MAB2457), rabbit anti-Pax2 (1:200,
744 Invitrogen, 71-6000), mouse anti-NeuN (1:100, Millipore, MAB377), rabbit anti-Calbindin
745 (1:1000, Millipore, AB1778), rabbit anti-Foxp2 (1:2000, Novus Biologicals NB100-55411),
746 chicken anti-Doublecortin: (1:100, Abcam ab153668). For immunofluorescence, secondary
747 antibodies (Invitrogen) labeled with fluorochrome were used to recognize the primary antibodies.

748

749 **Granule cell culture**

750 Granule cells were isolated and cultured as previously described (Lee et al., 2009). Briefly,
751 cerebella from litters of P6 mice were pooled and digested at 37 °C for 20 minutes in 10U ml⁻¹
752 papain (Worthington), and 250U ml⁻¹ DNase in EBSS using the Papain Dissociation Kit
753 (Worthington, Cat #:LK003150). The tissue was mechanically triturated and suspended cells
754 were isolated and resuspended in EBSS with albumin-ovomuroid inhibitor solution. Cell debris
755 was removed using a discontinuous density gradient and cells were resuspended in HBSS,
756 glucose and DNase. The cell suspension was then passed through a 40um cell strainer (Falcon
757 2340), layered on a step gradient of 35% and 65% Percoll (Sigma), and centrifuged at 2,500rpm
758 for 12 minutes at 25°C. Granule cells were harvested from the 35/65% interface and washed in
759 HBSS-glucose. Granule cells were then resuspended in Neurobasal medium and 10% FBS and
760 pre-plated on lightly coated poly-D-lysine-coated dishes for 20 minutes. This step allows any
761 heavier cells to drop and adhere to the coated surface while the granule cells are retained in the
762 media. Granule cells in the media were then collected, washed and counted using a
763 Hemocytometer. The cells were then plated on 25mm or 12mm poly-D-lysine (Sigma), laminin
764 coated coverglasses placed in 6-well plates with Neurobasal medium containing B-27 serum-free
765 supplement, 2mm l-glutamine, 100U/ml penicillin, and 100µg/ml streptomycin (pen-strep)
766 (Invitrogen, Grand Island, NY) and 0.45% d-glucose (Gibco). Granule cells were incubated at
767 37°C at 5% CO₂ were incubated for 3 days in vitro (DIV).
768 For aggregate cultures, aggregates were allowed to form by incubating purified granule cells for
769 20 hours on uncoated tissue culture dishes in DMEM containing 10% FBS, 0.45% D-glucose,

770 Pen-strep, 2mM L-glutamine at 4E6 cells/ml. Aggregates were then washed and cultured in
771 Neurobasal/B27 medium on poly-d-lysine/laminin-treated chamber slides at 37°C/5% CO₂.
772 Neuronal processes extend from aggregates and most form neurite bundles. After several hours,
773 small bipolar granule cells migrate unidirectionally away from the cell clusters along these
774 neurites and neurite bundles by extension of processes, followed by translocation of cell bodies
775 outside of the aggregate cell cluster margin. For immunofluorescence experiments, cells were
776 fixed in 4% paraformaldehyde for 10 minutes and washed with calcium and magnesium-free
777 PBS.

778

779 **RNA interference**

780 For the knockdown of Bhlhe22, we purchased ON-TARGETplus SMARTPool Mouse Bhlhe22
781 siRNA from Horizon Discovery (Cat ID: L-063262-01). Control samples were transfected with
782 ON-TARGETplus Non-targeting Control Pool (Cat ID: D-001810-10). siRNA molecules were
783 electroporated into isolated postnatal cerebellar granule cells using the Nucleofector 2b Device
784 (Lonza, AAB-1001) as previously described (Gartner et al., 2006). Briefly, after cells were
785 isolated (described above), 6-7E6 cells were resuspended in nucleofection solution and mixed
786 with 3µg of pCAG-EGFP plasmid (Addgene, 89684) and 600nM of siRNA. Cuvettes were
787 loaded with cellular solution and nucleofected using program O-03. After electroporation, cells
788 were allowed to recover in DMEM media in a humidified 37°C/5% CO₂ incubator for 90
789 minutes. Cells were washed and resuspended in either culture media for plating (dissociated
790 cultures) or DMEM media for overnight incubation (aggregate cultures).

791

792 **RNA isolation and reverse transcription followed by quantitative PCR (RT-qPCR)**

793 RNA was collected from cultured granule cells using the Monarch® Total RNA Miniprep Kit
794 (NEB). Then cDNA was reverse transcribed using SuperScript™ IV First-Strand Synthesis
795 System (Invitrogen) using random hexamers. Quantitative PCR was conducted using the Applied
796 Biosystems Fast SYBR Green Master Mix reagent and Applied Biosystems 7500 Real-time PCR
797 system. PCR conditions were as follows: 95 °C for 20 seconds, 40 cycles of 95 °C for 3 seconds,
798 and 60 °C for 30 seconds followed by 95 °C for 15 seconds, 60 °C for 1 minute, 95 °C for
799 15 seconds and 60 °C for 15 seconds. Three biological replicates were analyzed for each target
800 gene. Amplification of eGFP was used as a reference gene to normalize the relative amounts of

801 successfully transfected cells between treated and control experiments. Gene specific primers are
802 listed in Supplementary Table 4. Expression profiles for each gene were calculated using the
803 average relative quantity of the sample using the deltaCT method (Livak & Schmittgen, 2001). For
804 comparisons between siRNA treated and control samples, means were compared using a two-
805 tailed t-test. Results were expressed as the average \pm SE, and p-values <0.05 were considered
806 significant.

807

808 **Image analysis and microscopy**

809 Analysis and photomicroscopy were performed with a Zeiss Axiovert 200M microscope with the
810 AxioCam/AxioVision hardware-software components (Carl Zeiss) and downstream image
811 analysis was conducted using the AxioVision software v.4.9.1 (Carl Zeiss). For cerebellar
812 granule cell aggregate cultures, aggregate size determined using the tracing tool and all
813 aggregates analyzed were within 1000 squared microns of each other. Transfected cells were
814 identified by examining eGFP expression and for each biological replicate/experimental
815 treatment, 20 aggregates were examined. Granule cell migration was measured by calculating the
816 distance of migrated cells from the edge of the aggregate on captured images. Mean migration
817 distance was calculated for each aggregate, and the average of all 20 aggregates was used for
818 statistical analysis. The distribution of migrated cells from the aggregate was calculated for the
819 following ranges: $<25\mu\text{m}$, $25\text{-}50\mu\text{m}$, $50\text{-}75\mu\text{m}$, $75\text{-}100\mu\text{m}$, $>100\mu\text{m}$. For each range, the average
820 percentage was calculated for 20 aggregates per replicate. For comparisons between siRNA
821 treated and control samples, means were compared using a two-tailed t-test. Results were
822 expressed as the average \pm SE, and p-values <0.05 were considered significant.

823

824 **Plots and statistical methods**

825 All plots and correlation analysis were generated in R version 3.2.3 and figures were produced
826 using the package ggplot2. Bedtools v.2.28 (Quinlan & Hall, 2010) was used for comparing and
827 overlapping the genomic coordinates of peaks and existing genomic features described in the
828 manuscript. Boxplots represent the median (centre line), first and third quartiles (top and bottom
829 of box, respectively) and confidence intervals (95%; black lines). Genome browser screenshots
830 were taken from the IGV genome browser (Robinson et al., 2011). Bar plots results were
831 expressed as the average and the corresponding error bars represent standard error.

832

833 **GWAS SNP enrichment analysis**

834 Single nucleotide polymorphisms (SNPs) were retrieved from the GWAS Catalog (Buniello et al.,
835 2019) downloaded on March 8th, 2020. The SNPs were then filtered by their associated traits.
836 Traits containing the word “autism” were selected and from this list any traits containing the
837 word “or” were excluded. This resulted in a final list of 8 traits (Supplementary Table 2) and the
838 associated SNPs were used as input for our analysis. The software Genomic Regulatory
839 Elements and Gwas Overlap algoRithm (GREGOR) v.1.4.0 (Schmidt et al., 2015), a tool to test for
840 enrichment of an input list of trait-associated index SNPs in experimentally annotated regulatory
841 domains, was used to identify enrichment of trait-specific disease variants within enhancers. An
842 underlying hypothesis of GREGOR is that both trait-associated SNPs and variants in strong
843 linkage disequilibrium (LD) may be deemed as causal. For this, we used the European
844 population reference file (EUR; LD window size = 1 Mb; LD $r^2 \geq 0.7$) from 1000G data (Release
845 date: May 21, 2011). The probability of an overlap of either a SNP or at least one of its LD
846 proxies with our enhancers relative to a set of matched control variants was used to evaluate
847 significance of overlap. The enrichment p-value is the probability that the overlap of control
848 variants with our enhancers is greater than or equal to the overlap of the GWAS variants with our
849 enhancers.

850

851 ***De novo* mutation analysis**

852 *De novo* mutations were detected using whole-genome sequencing data from the MSSNG (Yuen
853 et al., 2016) and Simons Simplex Collection (SSC) (Isoda et al., 2017) cohorts using a pipeline
854 involving DeNovoGear (Ramu et al., 2013) as previously described (C Yuen et al., 2017). To
855 maximize data homogeneity, we included only individuals sequenced on the Illumina HiSeq X
856 platform. Individuals having a total DNM count more than three standard deviations above the
857 mean of the cohort were excluded. The NCBI LiftOver tool was used to convert the coordinates
858 of cerebellar enhancers from mm9 to hg19 to hg38, and BEDTools (Quinlan & Hall, 2010) was
859 used to identify DNMs overlapping these coordinates. Contingency tables (2x2) were generated
860 containing counts of the number of DNMs in ASD-affected individuals and unaffected siblings
861 either overlapping or not overlapping each dataset (cerebellar enhancer or H3K27ac peak
862 coordinates). Fisher’s exact test was used to determine statistical significance. Copy number

863 variants (CNVs) \geq 1000 bp were detected from the MSSNG and SSC WGS data using a
864 pipeline involving the algorithms ERDS (Zhu et al., 2012) and CNVnator (Abyzov, Urban, Snyder,
865 & Gerstein, 2011) as previously described (Trost et al., 2018). A CNV was deemed to be *de novo* if
866 it was detected by both ERDS and CNVnator in the child but by neither algorithm in both
867 parents. We then used BEDtools (Quinlan & Hall, 2010) to identify *de novo* CNVs overlapping
868 our cerebellar enhancers.

869 **Competing Interest Statement**

870 Authors have no competing interests.

871

872 **Author Contributions**

873 M.R. conducted experiments and was responsible for all major areas of concept formation, data
874 collection, analysis and manuscript composition. Y.B. processed and analyzed ChIP-seq data and
875 conducted the human variant enrichment analysis as well as contributed to manuscript writing.
876 J.Y. was involved in all mouse breeding and sample collection. J.W. and E.Y. were involved in
877 the initial profiling of Pax3 and conducting immunofluorescent experiments. B.T. and S.W.S.
878 conducted all genome-wide sequencing and analysis for the enrichment of autism spectrum
879 disorder variants. D.G. was the supervisory author and was involved in all areas of concept
880 formation and manuscript edits. All authors contributed to the final drafting of the manuscript.

881

882 **References**

- 883 Abyzov, A., Urban, A. E., Snyder, M., & Gerstein, M. (2011). CNVnator: An approach to
884 discover, genotype, and characterize typical and atypical CNVs from family and population
885 genome sequencing. *Genome Research*, 21(6), 974-984. doi:10.1101/gr.114876.110
- 886 Afgan, E., Baker, D., van den Beek, M., Blankenberg, D., Bouvier, D., Čech, M., . . . Goecks, J.
887 (2016). The galaxy platform for accessible, reproducible and collaborative biomedical
888 analyses: 2016 update. *Nucleic Acids Research*, 44(W1), W3-W10. doi:10.1093/nar/gkw343
- 889 Aruga, J., & Millen, K. J. (2018). ZIC1 function in normal cerebellar development and human
890 developmental pathology. *Advances in Experimental Medicine and Biology*, 1046, 249-268.
891 doi:10.1007/978-981-10-7311-3_13
- 892 Banerjee-Basu, S., & Packer, A. (2010). SFARI gene: An evolving database for the autism
893 research community. *Disease Models & Mechanisms*, 3(3-4), 133-135.
894 doi:10.1242/dmm.005439
- 895 Barešić, A., Nash, A. J., Dahoun, T., Howes, O., & Lenhard, B. (2020). Understanding the
896 genetics of neuropsychiatric disorders: The potential role of genomic regulatory blocks.
897 *Molecular Psychiatry*, 25(1), 6-18. doi:10.1038/s41380-019-0518-x

- 898 Ben-Arie, N., Bellen, H. J., Armstrong, D. L., McCall, A. E., Gordadze, P. R., Guo, Q., . . .
899 Zoghbi, H. Y. (1997). Math1 is essential for genesis of cerebellar granule neurons. *Nature*,
900 390(6656), 169-172. doi:10.1038/36579
- 901 Blankvoort, S., Witter, M. P., Noonan, J., Cotney, J., & Kentros, C. (2018). Marked diversity of
902 unique cortical enhancers enables neuron-specific tools by enhancer-driven gene expression.
903 *Current Biology: CB*, 28(13), 2103-2114.e5. doi:10.1016/j.cub.2018.05.015
- 904 Bonev, B., Mendelson Cohen, N., Szabo, Q., Fritsch, L., Papadopoulos, G. L., Lubling, Y., . . .
905 Cavalli, G. (2017). Multiscale 3D genome rewiring during mouse neural development. *Cell*,
906 171(3), 557-572.e24. doi:10.1016/j.cell.2017.09.043
- 907 Buniello, A., MacArthur, J. A. L., Cerezo, M., Harris, L. W., Hayhurst, J., Malangone, C., . . .
908 Parkinson, H. (2019). The NHGRI-EBI GWAS catalog of published genome-wide
909 association studies, targeted arrays and summary statistics 2019. *Nucleic Acids Research*,
910 47(D1), D1005-D1012. doi:10.1093/nar/gky1120 [doi]
- 911 C Yuen, R. K., Merico, D., Bookman, M., L Howe, J., Thiruvahindrapuram, B., Patel, R. V., . . .
912 Scherer, S. W. (2017). Whole genome sequencing resource identifies 18 new candidate
913 genes for autism spectrum disorder. *Nature Neuroscience*, 20(4), 602-611.
914 doi:10.1038/nn.4524
- 915 Calo, E., & Wysocka, J. (2013). Modification of enhancer chromatin: What, how, and why?
916 *Molecular Cell*, 49(5), 825-837. doi:10.1016/j.molcel.2013.01.038
- 917 Carter, R. A., Bihannic, L., Rosencrance, C., Hadley, J. L., Tong, Y., Phoenix, T. N., . . . Gawad,
918 C. (2018). A single-cell transcriptional atlas of the developing murine cerebellum. *Current*
919 *Biology: CB*, 28(18), 2910-2920.e2. doi:10.1016/j.cub.2018.07.062
- 920 Carullo, N. V. N., & Day, J. J. (2019). Genomic enhancers in brain health and disease. *Genes*,
921 10(1) doi:10.3390/genes10010043
- 922 Chilton, I., Okur, V., Vitiello, G., Selicorni, A., Mariani, M., Goldenberg, A., . . . Chung, W. K.
923 (2020). De novo heterozygous missense and loss-of-function variants in CDC42BPB are
924 associated with a neurodevelopmental phenotype. *American Journal of Medical Genetics.*
925 *Part A*, 182(5), 962-973. doi:10.1002/ajmg.a.61505
- 926 Consalez, G. G., Goldowitz, D., Casoni, F., & Hawkes, R. (2021). Origins, development, and
927 compartmentation of the granule cells of the cerebellum. *Frontiers in Neural Circuits*, 14
928 doi:10.3389/fncir.2020.611841
- 929 Creighton, M. P., Cheng, A. W., Welstead, G. G., Kooistra, T., Carey, B. W., Steine, E. J., . . .
930 Jaenisch, R. (2010). Histone H3K27ac separates active from poised enhancers and predicts
931 developmental state. *Proceedings of the National Academy of Sciences of the United States*
932 *of America*, 107(50), 21931-21936. doi:10.1073/pnas.1016071107

- 933 de la Torre-Ubieta, L., Stein, J. L., Won, H., Opland, C. K., Liang, D., Lu, D., & Geschwind, D.
934 H. (2018). The dynamic landscape of open chromatin during human cortical neurogenesis.
935 *Cell*, 172(1-2), 289-304.e18. doi:10.1016/j.cell.2017.12.014
- 936 Dixon, J. R., Selvaraj, S., Yue, F., Kim, A., Li, Y., Shen, Y., . . . Ren, B. (2012). Topological
937 domains in mammalian genomes identified by analysis of chromatin interactions. *Nature*,
938 485(7398), 376-380. doi:10.1038/nature11082
- 939 Ebner, B. A., Ingram, M. A., Barnes, J. A., Duvick, L. A., Frisch, J. L., Clark, H. B., . . . Orr, H.
940 T. (2013). Purkinje cell ataxin-1 modulates climbing fiber synaptic input in developing and
941 adult mouse cerebellum. *The Journal of Neuroscience: The Official Journal of the Society*
942 *for Neuroscience*, 33(13), 5806-5820. doi:10.1523/JNEUROSCI.6311-11.2013
- 943 Elsen, G. E., Bedogni, F., Hodge, R. D., Bammler, T. K., MacDonald, J. W., Lindtner, S., . . .
944 Hevner, R. F. (2018). The epigenetic factor landscape of developing neocortex is regulated
945 by transcription factors Pax6→ Tbr2→ Tbr1. *Frontiers in Neuroscience*, 12, 571.
946 doi:10.3389/fnins.2018.00571
- 947 Fischbach, G. D., & Lord, C. (2010). The simons simplex collection: A resource for
948 identification of autism genetic risk factors. *Neuron*, 68(2), 192-195.
949 doi:10.1016/j.neuron.2010.10.006
- 950 Frank, C. L., Liu, F., Wijayatunge, R., Song, L., Biegler, M. T., Yang, M. G., . . . West, A. E.
951 (2015). Regulation of chromatin accessibility and zic binding at enhancers in the developing
952 cerebellum. *Nature Neuroscience*, 18(5), 647-656. doi:10.1038/nn.3995
- 953 Frantz, G. D., Bohner, A. P., Akers, R. M., & McConnell, S. K. (1994). Regulation of the POU
954 domain gene SCIP during cerebral cortical development. *The Journal of Neuroscience: The*
955 *Official Journal of the Society for Neuroscience*, 14(2), 472-485.
- 956 Fujita, E., Tanabe, Y., Shiota, A., Ueda, M., Suwa, K., Momoi, M. Y., & Momoi, T. (2008).
957 Ultrasonic vocalization impairment of Foxp2 (R552H) knockin mice related to speech-
958 language disorder and abnormality of purkinje cells. *Proceedings of the National Academy*
959 *of Sciences of the United States of America*, 105(8), 3117-3122.
960 doi:10.1073/pnas.0712298105
- 961 Gao, T., & Qian, J. (2020). EnhancerAtlas 2.0: An updated resource with enhancer annotation in
962 586 tissue/cell types across nine species. *Nucleic Acids Research*, 48(D1), D58-D64.
963 doi:10.1093/nar/gkz980 [doi]
- 964 Gartner, A., Collin, L., & Lalli, G. (2006). Nucleofection of primary neurons. *Methods in*
965 *Enzymology*, 406, 374-388. doi:S0076-6879(06)06027-7 [pii]
- 966 Goldowitz, D., & Hamre, K. (1998). The cells and molecules that make a cerebellum. *Trends in*
967 *Neurosciences*, 21(9), 375-382.

- 968 Grove, J., Ripke, S., Als, T. D., Mattheisen, M., Walters, R. K., Won, H., . . . Børglum, A. D.
969 (2019). Identification of common genetic risk variants for autism spectrum disorder. *Nature*
970 *Genetics*, *51*(3), 431-444. doi:10.1038/s41588-019-0344-8
- 971 Heinz, S., Benner, C., Spann, N., Bertolino, E., Lin, Y. C., Laslo, P., . . . Glass, C. K. (2010).
972 Simple combinations of lineage-determining transcription factors prime cis-regulatory
973 elements required for macrophage and B cell identities. *Molecular Cell*, *38*(4), 576-589.
974 doi:10.1016/j.molcel.2010.05.004 [doi]
- 975 Heinz, S., Romanoski, C. E., Benner, C., & Glass, C. K. (2015). The selection and function of
976 cell type-specific enhancers. *Nature Reviews. Molecular Cell Biology*, *16*(3), 144-154.
977 doi:10.1038/nrm3949
- 978 Hoshino, M., Nakamura, S., Mori, K., Kawauchi, T., Terao, M., Nishimura, Y. V., . . .
979 Nabeshima, Y. (2005). Ptf1a, a bHLH transcriptional gene, defines GABAergic neuronal
980 fates in cerebellum. *Neuron*, *47*(2), 201-213. doi:10.1016/j.neuron.2005.06.007
- 981 Isoda, T., Moore, A. J., He, Z., Chandra, V., Aida, M., Denholtz, M., . . . Murre, C. (2017). Non-
982 coding transcription instructs chromatin folding and compartmentalization to dictate
983 enhancer-promoter communication and T cell fate. *Cell*, *171*(1), 103-119.e18.
984 doi:10.1016/j.cell.2017.09.001
- 985 Joshi, P. S., Molyneaux, B. J., Feng, L., Xie, X., Macklis, J. D., & Gan, L. (2008). Bhlhb5
986 regulates the postmitotic acquisition of area identities in layers II-V of the developing
987 neocortex. *Neuron*, *60*(2), 258-272. doi:10.1016/j.neuron.2008.08.006
- 988 Kevin Blighe, Sharmila Rana, & Myles Lewis. (2020). EnhancedVolcano: Publication-ready
989 volcano plots with enhanced colouring and labeling [computer software]
- 990 Kim, E. J., Battiste, J., Nakagawa, Y., & Johnson, J. E. (2008). Ascl1 (Mash1) lineage cells
991 contribute to discrete cell populations in CNS architecture. *Molecular and Cellular*
992 *Neurosciences*, *38*(4), 595-606. doi:10.1016/j.mcn.2008.05.008 [doi]
- 993 Klisch, T. J., Xi, Y., Flora, A., Wang, L., Li, W., & Zoghbi, H. Y. (2011). In vivo Atoh1
994 targetome reveals how a proneural transcription factor regulates cerebellar development.
995 *Proceedings of the National Academy of Sciences*, *108*(8), 3288-3293.
- 996 Koziol, L. F., Budding, D., Andreasen, N., D'Arrigo, S., Bulgheroni, S., Imamizu, H., . . .
997 Yamazaki, T. (2014). Consensus paper: The cerebellum's role in movement and cognition.
998 *Cerebellum (London, England)*, *13*(1), 151-177. doi:10.1007/s12311-013-0511-x
- 999 Langmead, B., Trapnell, C., Pop, M., & Salzberg, S. L. (2009). Ultrafast and memory-efficient
1000 alignment of short DNA sequences to the human genome. *Genome Biology*, *10*(3), R25.
1001 doi:10.1186/gb-2009-10-3-r25

- 1002 Lee, H. Y., Greene, L. A., Mason, C. A., & Manzini, M. C. (2009). Isolation and culture of post-
1003 natal mouse cerebellar granule neuron progenitor cells and neurons. *Journal of Visualized*
1004 *Experiments : JoVE*, (23). pii: 990. doi(23), 10.3791/990. doi:10.3791/990 [doi]
- 1005 Leto, K., Bartolini, A., Yanagawa, Y., Obata, K., Magrassi, L., Schilling, K., & Rossi, F. (2009).
1006 Laminar fate and phenotype specification of cerebellar GABAergic interneurons. *The*
1007 *Journal of Neuroscience: The Official Journal of the Society for Neuroscience*, 29(21),
1008 7079-7091. doi:10.1523/JNEUROSCI.0957-09.2009
- 1009 Leto, K., Carletti, B., Williams, I. M., Magrassi, L., & Rossi, F. (2006). Different types of
1010 cerebellar GABAergic interneurons originate from a common pool of multipotent progenitor
1011 cells. *The Journal of Neuroscience: The Official Journal of the Society for Neuroscience*,
1012 26(45), 11682-11694. doi:10.1523/JNEUROSCI.3656-06.2006
- 1013 Limperopoulos, C., Chilingaryan, G., Sullivan, N., Guizard, N., Robertson, R. L., & du Plessis,
1014 A. J. (2014). Injury to the premature cerebellum: Outcome is related to remote cortical
1015 development. *Cerebral Cortex (New York, N.Y.: 1991)*, 24(3), 728-736.
1016 doi:10.1093/cercor/bhs354
- 1017 Lindtner, S., Catta-Preta, R., Tian, H., Su-Feher, L., Price, J. D., Dickel, D. E., . . . Rubenstein, J.
1018 L. R. (2019). Genomic resolution of DLX-orchestrated transcriptional circuits driving
1019 development of forebrain GABAergic neurons. *Cell Reports*, 28(8), 2048-2063.e8.
1020 doi:10.1016/j.celrep.2019.07.022
- 1021 Lister, R., Mukamel, E. A., Nery, J. R., Urich, M., Puddifoot, C. A., Johnson, N. D., . . . Ecker, J.
1022 R. (2013). Global epigenomic reconfiguration during mammalian brain development.
1023 *Science (New York, N.Y.)*, 341(6146), 1237905. doi:10.1126/science.1237905
- 1024 Livak, K. J., & Schmittgen, T. D. (2001). Analysis of relative gene expression data using real-
1025 time quantitative PCR and the 2(-delta delta C(T)) method. *Methods (San Diego, Calif.)*,
1026 25(4), 402-408. doi:10.1006/meth.2001.1262 [doi]
- 1027 Lorzadeh, A., Lopez Gutierrez, R., Jackson, L., Moksa, M., & Hirst, M. (2017). Generation of
1028 native chromatin immunoprecipitation sequencing libraries for nucleosome density analysis.
1029 *Journal of Visualized Experiments : JoVE*, (130). doi(130), 10.3791/56085.
1030 doi:10.3791/56085 [doi]
- 1031 Maricich, S. M., & Herrup, K. (1999). Pax-2 expression defines a subset of GABAergic
1032 interneurons and their precursors in the developing murine cerebellum. *Journal of*
1033 *Neurobiology*, 41(2), 281-294. doi:10.1002/(sici)1097-4695(19991105)41:23.0.co;2-5
- 1034 Miyata, T., Maeda, T., & Lee, J. E. (1999). NeuroD is required for differentiation of the granule
1035 cells in the cerebellum and hippocampus. *Genes & Development*, 13(13), 1647-1652.
1036 doi:10.1101/gad.13.13.1647

- 1037 Nord, A. S., Blow, M. J., Attanasio, C., Akiyama, J. A., Holt, A., Hosseini, R., . . . Visel, A.
1038 (2013). Rapid and pervasive changes in genome-wide enhancer usage during mammalian
1039 development. *Cell*, *155*(7), 1521-1531. doi:10.1016/j.cell.2013.11.033
- 1040 Nord, A. S., & West, A. E. (2020). Neurobiological functions of transcriptional enhancers.
1041 *Nature Neuroscience*, *23*(1), 5-14. doi:10.1038/s41593-019-0538-5
- 1042 Nott, A., Holtman, I. R., Coufal, N. G., Schlachetzki, J. C. M., Yu, M., Hu, R., . . . Glass, C. K.
1043 (2019). Brain cell type-specific enhancer-promoter interactome maps and disease-risk
1044 association. *Science (New York, N.Y.)*, *366*(6469), 1134-1139. doi:10.1126/science.aay0793
- 1045 Osterwalder, M., Barozzi, I., Tissières, V., Fukuda-Yuzawa, Y., Mannion, B. J., Afzal, S. Y., . . .
1046 Pennacchio, L. A. (2018). Enhancer redundancy provides phenotypic robustness in
1047 mammalian development. *Nature*, *554*(7691), 239-243. doi:10.1038/nature25461
- 1048 Pattabiraman, K., Golonzhka, O., Lindtner, S., Nord, A. S., Taher, L., Hoch, R., . . . Rubenstein,
1049 J. L. R. (2014). Transcriptional regulation of enhancers active in protodomains of the
1050 developing cerebral cortex. *Neuron*, *82*(5), 989-1003. doi:10.1016/j.neuron.2014.04.014
- 1051 Peng, J., Sheng, A., Xiao, Q., Shen, L., Ju, X., Zhang, M., . . . Luo, Z. (2019). Single-cell
1052 transcriptomes reveal molecular specializations of neuronal cell types in the developing
1053 cerebellum. *Journal of Molecular Cell Biology*, doi:10.1093/jmcb/mjy089
- 1054 Pichaud, F., Walther, R. F., & Nunes de Almeida, F. (2019). Regulation of Cdc42 and its
1055 effectors in epithelial morphogenesis. *Journal of Cell Science*, *132*(10)
1056 doi:10.1242/jcs.217869
- 1057 Porter, F. D., Drago, J., Xu, Y., Cheema, S. S., Wassif, C., Huang, S. P., . . . Westphal, H.
1058 (1997). Lhx2, a LIM homeobox gene, is required for eye, forebrain, and definitive
1059 erythrocyte development. *Development (Cambridge, England)*, *124*(15), 2935-2944.
- 1060 Preissl, S., Fang, R., Huang, H., Zhao, Y., Raviram, R., Gorkin, D. U., . . . Ren, B. (2018).
1061 Single-nucleus analysis of accessible chromatin in developing mouse forebrain reveals cell-
1062 type-specific transcriptional regulation. *Nature Neuroscience*, *21*(3), 432-439.
1063 doi:10.1038/s41593-018-0079-3
- 1064 Quinlan, A. R., & Hall, I. M. (2010). BEDTools: A flexible suite of utilities for comparing
1065 genomic features. *Bioinformatics (Oxford, England)*, *26*(6), 841-842.
1066 doi:10.1093/bioinformatics/btq033
- 1067 Ramírez, F., Ryan, D. P., Grüning, B., Bhardwaj, V., Kilpert, F., Richter, A. S., . . . Manke, T.
1068 (2016). deepTools2: A next generation web server for deep-sequencing data analysis.
1069 *Nucleic Acids Research*, *44*(W1), 160. doi:10.1093/nar/gkw257

- 1070 Ramu, A., Noordam, M. J., Schwartz, R. S., Wuster, A., Hurles, M. E., Cartwright, R. A., &
1071 Conrad, D. F. (2013). DeNovoGear: De novo indel and point mutation discovery and
1072 phasing. *Nature Methods*, *10*(10), 985-987. doi:10.1038/nmeth.2611
- 1073 Rinaldi, A., Defterali, C., Mialot, A., Garden, D. L. F., Beraneck, M., & Nolan, M. F. (2013).
1074 HCN1 channels in cerebellar purkinje cells promote late stages of learning and constrain
1075 synaptic inhibition. *The Journal of Physiology*, *591*(22), 5691-5709.
1076 doi:10.1113/jphysiol.2013.259499
- 1077 Robinson, J. T., Thorvaldsdottir, H., Winckler, W., Guttman, M., Lander, E. S., Getz, G., &
1078 Mesirov JP, -. e. (2011). Integrative genomics viewer. *Nature Biotechnology*, *29*(1), 24-26.
1079 doi:10.1038/nbt.1754 [doi]
- 1080 Sanchez-Ortiz, E., Cho, W., Nazarenko, I., Mo, W., Chen, J., & Parada, L. F. (2014). NF1
1081 regulation of RAS/ERK signaling is required for appropriate granule neuron progenitor
1082 expansion and migration in cerebellar development. *Genes & Development*, *28*(21), 2407-
1083 2420. doi:10.1101/gad.246603.114
- 1084 Sarropoulos, I., Sepp, M., Frömel, R., Leiss, K., Trost, N., Leushkin, E., . . . Kaessmann, H.
1085 (2021). The regulatory landscape of cells in the developing mouse cerebellum. *bioRxiv*, ,
1086 2021.01.29.428632. doi:10.1101/2021.01.29.428632
- 1087 Schmidt, E. M., Zhang, J., Zhou, W., Chen, J., Mohlke, K. L., Chen, Y. E., & Willer, C. J.
1088 (2015). GREGOR: Evaluating global enrichment of trait-associated variants in epigenomic
1089 features using a systematic, data-driven approach. *Bioinformatics (Oxford, England)*,
1090 *31*(16), 2601-2606. doi:10.1093/bioinformatics/btv201 [doi]
- 1091 Stark, R., & Brown, G. (2011). DiffBind: Differential binding analysis of ChIP-seq peak
1092 data.[computer software]
- 1093 Stoodley, C. J., & Limperopoulos, C. (2016). Structure-function relationships in the developing
1094 cerebellum: Evidence from early-life cerebellar injury and neurodevelopmental disorders.
1095 *Seminars in Fetal & Neonatal Medicine*, *21*(5), 356-364. doi:10.1016/j.siny.2016.04.010
- 1096 Su, X., Liu, X., Ni, L., Shi, W., Zhu, H., Shi, J., . . . Huang, Q. (2016). GFAP expression is
1097 regulated by Pax3 in brain glioma stem cells. *Oncology Reports*, *36*(3), 1277-1284.
1098 doi:10.3892/or.2016.4917
- 1099 Swanson, D. J., & Goldowitz, D. (2011). Experimental sey mouse chimeras reveal the
1100 developmental deficiencies of Pax6-null granule cells in the postnatal cerebellum.
1101 *Developmental Biology*, *351*(1), 1-12. doi:10.1016/j.ydbio.2010.11.018
- 1102 Takács, J., Zaninetti, R., Vig, J., Vastagh, C., & Hámori, J. (2008). Postnatal expression of
1103 doublecortin (dcx) in the developing cerebellar cortex of mouse. *Acta Biologica Hungarica*,
1104 *59*(2), 147-161. doi:10.1556/ABiol.59.2008.2.2

- 1105 Thompson, C. L., Ng, L., Menon, V., Martinez, S., Lee, C., Glattfelder, K., . . . Jones, A. R.
1106 (2014). A high-resolution spatiotemporal atlas of gene expression of the developing mouse
1107 brain. *Neuron*, *83*(2), 309-323. doi:10.1016/j.neuron.2014.05.033
- 1108 Trost, B., Walker, S., Wang, Z., Thiruvahindrapuram, B., MacDonald, J. R., Sung, W. W. L., . . .
1109 Scherer, S. W. (2018). A comprehensive workflow for read depth-based identification of
1110 copy-number variation from whole-genome sequence data. *American Journal of Human*
1111 *Genetics*, *102*(1), 142-155. doi:10.1016/j.ajhg.2017.12.007
- 1112 Umeda, T., Takashima, N., Nakagawa, R., Maekawa, M., Ikegami, S., Yoshikawa, T., . . .
1113 Osumi, N. (2010). Evaluation of Pax6 mutant rat as a model for autism. *PloS One*, *5*(12),
1114 e15500. doi:10.1371/journal.pone.0015500
- 1115 Urbánek, P., Fetka, I., Meisler, M. H., & Busslinger, M. (1997). Cooperation of Pax2 and Pax5
1116 in midbrain and cerebellum development. *Proceedings of the National Academy of Sciences*
1117 *of the United States of America*, *94*(11), 5703-5708. doi:10.1073/pnas.94.11.5703
- 1118 Visel, A., Minovitsky, S., Dubchak, I., & Pennacchio, L. A. (2007). VISTA enhancer browser--a
1119 database of tissue-specific human enhancers. *Nucleic Acids Research*, *35*(Database issue),
1120 88. doi:10.1093/nar/gkl822
- 1121 Visel, A., Rubin, E. M., & Pennacchio, L. A. (2009). Genomic views of distant-acting enhancers.
1122 *Nature*, *461*(7261), 199-205. doi:10.1038/nature08451
- 1123 Visel, A., Taher, L., Girgis, H., May, D., Golonzhka, O., Hoch, R. V., . . . Rubenstein, J. L. R.
1124 (2013). A high-resolution enhancer atlas of the developing telencephalon. *Cell*, *152*(4), 895-
1125 908. doi:10.1016/j.cell.2012.12.041
- 1126 Wang, V. Y., & Zoghbi, H. Y. (2001). Genetic regulation of cerebellar development. *Nature*
1127 *Reviews. Neuroscience*, *2*(7), 484-491. doi:10.1038/35081558
- 1128 Wang, W., Mullikin-Kilpatrick, D., Crandall, J. E., Gronostajski, R. M., Litwack, E. D., &
1129 Kilpatrick, D. L. (2007). Nuclear factor I coordinates multiple phases of cerebellar granule
1130 cell development via regulation of cell adhesion molecules. *Journal of Neuroscience*,
1131 *27*(23), 6115-6127.
- 1132 Weyer, A., & Schilling, K. (2003). Developmental and cell type-specific expression of the
1133 neuronal marker NeuN in the murine cerebellum. *Journal of Neuroscience Research*, *73*(3),
1134 400-409. doi:10.1002/jnr.10655
- 1135 Whyte, W. A., Bilodeau, S., Orlando, D. A., Hoke, H. A., Frampton, G. M., Foster, C. T., . . .
1136 Young, R. A. (2012). Enhancer decommissioning by LSD1 during embryonic stem cell
1137 differentiation. *Nature*, *482*(7384), 221-225. doi:10.1038/nature10805
- 1138 Wizeman, J. W., Guo, Q., Wilion, E. M., & Li, J. Y. (2019). Specification of diverse cell types
1139 during early neurogenesis of the mouse cerebellum. *eLife*, *8* doi:10.7554/eLife.42388

- 1140 Yao, P., Lin, P., Gokoolparsadh, A., Assareh, A., Thang, M. W., & Voineagu, I. (2015).
1141 Coexpression networks identify brain region-specific enhancer RNAs in the human brain.
1142 *Nature Neuroscience*, *18*(8), 1168-1174. doi:10.1038/nn.4063 [doi]
- 1143 Yeung, J., Ha, T. J., Swanson, D. J., & Goldowitz, D. (2016a). A novel and multivalent role of
1144 Pax6 in cerebellar development. *The Journal of Neuroscience: The Official Journal of the*
1145 *Society for Neuroscience*, *36*(35), 9057-9069. doi:10.1523/JNEUROSCI.4385-15.2016
- 1146 Yeung, J., Ha, T. J., Swanson, D. J., & Goldowitz, D. (2016b). A novel and multivalent role of
1147 Pax6 in cerebellar development. *The Journal of Neuroscience: The Official Journal of the*
1148 *Society for Neuroscience*, *36*(35), 9057-9069. doi:10.1523/JNEUROSCI.4385-15.2016
- 1149 Yuen, R. K. C., Merico, D., Cao, H., Pellecchia, G., Alipanahi, B., Thiruvahindrapuram, B., . . .
1150 Scherer, S. W. (2016). Genome-wide characteristics of de novo mutations in autism. *NPJ*
1151 *Genomic Medicine*, *1*, 160271-1602710. doi:10.1038/npjgenmed.2016.27
- 1152 Zhang, D., Stumpo, D. J., Graves, J. P., DeGraff, L. M., Grissom, S. F., Collins, J. B., . . .
1153 Blackshear, P. J. (2006). Identification of potential target genes for RFX4_v3, a
1154 transcription factor critical for brain development. *Journal of Neurochemistry*, *98*(3), 860-
1155 875. doi:10.1111/j.1471-4159.2006.03930.x
- 1156 Zhang, P. G. Y., Yeung, J., Gupta, I., Ramirez, M., Ha, T., Swanson, D. J., . . . Goldowitz, D.
1157 (2018). Discovery of transcription factors novel to mouse cerebellar granule cell
1158 development through laser-capture microdissection. *Cerebellum (London, England)*,
1159 doi:10.1007/s12311-017-0912-3
- 1160 Zhang, Y., Liu, T., Meyer, C. A., Eeckhoutte, J., Johnson, D. S., Bernstein, B. E., . . . Liu, X. S.
1161 (2008). Model-based analysis of ChIP-seq (MACS). *Genome Biology*, *9*(9), R137.
1162 doi:10.1186/gb-2008-9-9-r137
- 1163 Zhao, Y., Kwan, K., Mailloux, C. M., Lee, W., Grinberg, A., Wurst, W., . . . Westphal, H.
1164 (2007). LIM-homeodomain proteins Lhx1 and Lhx5, and their cofactor Ldb1, control
1165 purkinje cell differentiation in the developing cerebellum. *Proceedings of the National*
1166 *Academy of Sciences of the United States of America*, *104*(32), 13182-13186.
1167 doi:10.1073/pnas.0705464104
- 1168 Zhu, M., Need, A. C., Han, Y., Ge, D., Maia, J. M., Zhu, Q., . . . Goldstein, D. B. (2012). Using
1169 ERDS to infer copy-number variants in high-coverage genomes. *American Journal of*
1170 *Human Genetics*, *91*(3), 408-421. doi:10.1016/j.ajhg.2012.07.004
- 1171 Ziats, M. N., Grosvenor, L. P., & Rennert, O. M. (2015). Functional genomics of human brain
1172 development and implications for autism spectrum disorders. *Translational Psychiatry*, *5*,
1173 e665. doi:10.1038/tp.2015.153